INSTITUTO POLITÉCNICO DE BRAGANÇA
Escola Superior de Tecnologia e Gestão

Experimental and Numerical study of a Diffuser Augmented Wind Turbine - DAWT

Lino André Bala Maia

Dissertation final report submitted to
Escola Superior de Tecnologia e de Gestão
Instituto Politécnico de Bragança

for the Master's Degree of
Renewable Energies and Energy Efficiency

December 2014

Experimental and Numerical study of a Diffuser Augmented Wind Turbine - DAWT

Lino André Bala Maia

Dissertation final report submitted to
Escola Superior de Tecnologia e de Gestão
Instituto Politécnico de Bragança

for the Master's Degree of
Renewable Energies and Energy Efficiency

Supervisors:

Professor Luís Frölén Ribeiro
Professor João Eduardo Ribeiro

December 2014

Acknowledgments

I would like to express my sincere gratitude to my supervisors Professor Luís Frölén Ribeiro and Professor João Eduardo Ribeiro for their support, the scientific guidance and the encouragement given during this dissertation.

I would like to greatly thank Professor Luis Frölén Ribeiro, who gave me the opportunity to work in the *Enhanced WT* project.

I am very grateful to Professor João Eduardo Ribeiro for the transmitted knowledge and interest in Computational Fluid Dynamics.

My grateful acknowledge to Escola Superior de Tecnologia e Gestão (ESTiG) directed by Professor Albano Alves for providing the conditions and equipment needed.

This work would not be possible without the help of colleague Jorge Paulo. I am grateful for the support and patience that he showed in my research activities.

Also i thank my *Enhanced WT* colleagues for the companionship and cooperation provided.

Finally, I would thank my parents, and a devote thanks to Sofia, for her love and support.

Abstract

The effect of concentrator-diffuser (C-D) of a shrouded wind turbine was studied. The main objective involved assessing the increment that this device induces in productivity of small wind turbines. Also the aerodynamic performance of two scaled blade models were studied in terms of drag and lift forces as a function of angle of attack for *Re* of 15714 and 37143.

Wind turbine power performance was evaluated in terms of power coefficient values. Laboratory measurements showed that improvements were obtained on the electrical power values, resulting in an average increase of 90% in the corresponding power coefficient values. A more pronounced enhancement is described at lower wind speed values.

CFD calculations were performed at flow values of 6 and 14 m/s to the C-D device. CFD calculations performed an evaluation of velocity experienced in the action rotor zone, which provided maximum increases of 81 % and 86 %, respectively.

Numerical simulations and experimental measurements were performed also to the blades, where the results obtained were similar, providing a difference of 25 % for drag forces.

Keywords: Concentrator-diffuser; blade aerodynamic; small wind turbine; power coefficient.

Resumo

Neste trabalho estudou-se o efeito do concentrador-difusor (C-D) numa turbina eólica encapsulada. O principal objetivo deste estudo é avaliar o incremento que o C-D induz na produtividade de turbinas eólicas de pequena dimensão. Foi também avaliado o desempenho aerodinâmico de dois modelos de uma pá com diferentes razões de escala. Estes modelos foram avaliados em termos de forças de arrasto e de sustentação em função do ângulo de ataque, considerando Reynolds de 15714 e 37143.

O desempenho energético da turbina foi avaliada em termos de coeficiente de potência. Segundo as medições laboratoriais verificou-se melhorias nos valores de potência elétrica, resultando num aumento médio de 90 %, nos correspondentes valores de coeficiente de potência. Para valores de velocidade mais baixos verificou-se um incremente mais pronunciado.

Efetuaram-se simulações CFD ao dispositivo C-D para valores de velocidade de vento de 6 e 14 m/s. Estas simulações reproduziram uma avaliação dos valores de velocidade do ar verificados na zona de ação do rotor, produzindo aumentos máximos de 81 % e 86 %, respetivamente.

Aplicaram-se também medições experimentais e simulações numéricas para avaliar o desempenho aerodinâmico da pá. Estas produziram resultados similares, originando uma diferença média de 25 % nos valores das forças de arrasto.

Palavras-chave: Concentrador-difusor; aerodinâmica da pá; pequena turbina eólica; coeficiente de potência

Contents

1 Introduction **1**

1.1 Motivation and Objectives 1
1.2 State of the Art 1
1.3 Structure 7

2 Literature Review **9**

2.1 Wind Turbine Aerodynamics 9
2.1.1 Actuator Disc Model and Betz Limit 9
2.1.2 Effects of Wake Rotation on Betz Limit 12
2.1.3 Theoretical Analysis of Shrouded Rotor 15
2.1.4 Forces Acting on a Blades 17
2.1.5 Airfoils 19
2.1.6 Blade Element Theory 20
2.2 Numerical Simulation (CFD) 22
2.2.1 Governing Equations 23
2.2.2 Structure of CFD Code 24
2.2.3 Grid Generation 25
2.2.4 Finite-Volume Method 25
2.2.5 Turbulence Modeling 26
2.2.5.1 k - ε Model 27
2.2.5.2 k - ω Model 30

3 Methodology **31**

3.1 Experimental 31
3.1.1 Blade Aerodynamics 31
3.1.2 Wind Turbine Performance 34
3.2 Numerical Methodology 37
3.2.1 Blade Aerodynamics 37
3.2.1.1 Pre-Solver 37
3.2.1.2 Solver 40
3.2.2 Wind Turbine Performance 41

3.2.2.1 Pre-Solver 41
3.2.2.2 Solver 44

4 Results and Discussions **47**
4.1 Experimental 47
4.1.1 Blade Aerodynamics 47
4.1.2 Wind Turbine Performance 49
4.2 Numerical Simulations 55
4.2.1 Blade Aerodynamics 55
4.2.2 Wind Turbine Performance 60
4.3 Experimental vs CFD 65

5 Conclusions **71**
5.1 Conclusions 71
5.2 Future Works 72

List of Figures

1.1 Schematic system representation composed by a concentrator-diffuser (C-D) and a wind turbine (WT), developed by Paulo (2013). 5
1.2 *Enhanced WT* prototype tested at 12 meters in unbuilt environment. . . . 6

2.1 Actuator disk model of a wind turbine, adapted from (Jonkman 2003, Manwell et al. 2002). 10
2.2 Wake rotation structure (Jonkman 2003). 13
2.3 Theoretical maximum power coefficient as function of tip speed ratio for an ideal HAWT, with and without wake rotation, adapted from Eggleston & Stoddard (1987). 14
2.4 Theoretical power coefficients (C_P) of wind rotors considering different designs as function of tip speed ratio (λ) (Wilson & Lissaman 1974, Hau 2006). 14
2.5 Schematic representation of systems that concentrate and accelerate the wind, adapted from Ohya et al. (2008). 15
2.6 Representative illustration of the flow around the shroud, considering the presence of brim, adapted from Ohya & Karasudani (2010). 17
2.7 Resultant forces acting on an airfoil (Jonkman 2003). 18
2.8 Pressure distribution around an airfoil (Vennard et al. 1996). 19
2.9 Airfoil nomenclature (Anderson 2001). 19
2.10 Blade element model, divided into dr section (Kulunk 2011). 20
2.11 Blade geometry (cross section) for analysis of blade element theory (Jonkman 2003). 21

3.1 Subsonic Wind Tunnel. 32
3.2 Aerodynamic models produced considering a different scaling factor. . . . 33
3.3 Wind turbine model used in experimental setup. 35
3.4 Electrical circuit diagram used to evaluate electric power generated. . . . 35
3.5 C-D system used in experimental trials. 36
3.6 Representation of the model developed by Paulo (2013), implemented in experimental wind tunnel setup. 36

3.7 Mesh of blade computational domain, without the presence of virtual wind tunnel structure. 38
3.8 Computational domain and boundary conditions. 39
3.9 Computational domain produced with the enclosed wind turbine (B1 - velocity-inlet and B2 - pressure-outlet). 41
3.10 Computational domain specifications, WT distance relative to velocity-inlet (B1) and with pressure-outlet (B2). 42
3.11 Computational mesh generated for the analysis of rotor performance. . . . 42
3.12 Computational domain produced with the enclosed C-D (B1 - velocity-inlet and B2 - pressure-outlet). 43
3.13 Computational mesh performed for the analysis of effects that C-D generated in air flow. 44

4.1 Experimental electric power generated by the aerodynamic model in wind tunnel trials. 50
4.2 Errorbar graph of rotor rotational speeds obtained relative to those described in Paulo (2013). 51
4.3 Wind Turbine power coefficient performance as function of different wind speed values. 51
4.4 Experimental electric power generated by the implementation of shroud in wind tunnel trials ($\triangle$) compared to those described in Paulo (2013) ($*$) . 52
4.5 Electric power values in function of wind speed, in the case of Wind Turbine ($*$) and Wind Turbine adapted with a Convergent-Diffuser ($\triangle$). . . . 53
4.6 Evaluation of power coefficient performance performed to the Wind Turbine ($*$) and Wind Turbine combined with Concentrator-Diffuser ($\triangle$) in function of wind speed values. 54
4.7 Computed Pressure Coefficient distributions on the aerodynamic model blade 2. 56
4.8 Computed Pressure Coefficient distributions on the aerodynamic model blade 1. 57
4.9 Blade surface turbulence kinetic energy plots overlaid with surface streamlines, for blade model 2. 58
4.10 Blade surface turbulence kinetic energy plots overlaid with surface streamlines, for blade model 1. 59
4.11 Computed wind turbine power coefficient performance as function of different wind speed values. 61
4.12 Streamline of air flow velocity that surrounds C-D device, considering an approaching wind speed of 6 m/s. 62

4.13 Streamline of air flow velocity that surrounds C-D device, considering an approaching wind speed of 14 m/s. 62
4.14 Radial contour of velocity experienced at rotor acting zone in C-D device, pondering an approaching wind of 6 m/s. 63
4.15 Radial contour of velocity experienced at rotor acting zone in C-D device, pondering an approaching wind of 14 m/s. 63
4.16 Turbulence generated at C-D outflow, evaluated in terms of turbulence kinetic energy, considering an approaching wind of 6 m/s. 64
4.17 Turbulence generated at C-D outflow, evaluated in terms of turbulence kinetic energy, considering an approaching wind of 14 m/s. 64
4.18 Drag force relative to the aerodynamic blade model 1 in function of attack angle variation. 65
4.19 Lift force relative to the aerodynamic blade model 1 in function of attack angle variation. 66
4.20 Drag force relative to the aerodynamic model blade 2 in function of attack angle variation. 67
4.21 Lift force relative to the aerodynamic blade model 2 in function of attack angle variation. 68
4.22 Power coefficient confrontation through experimental (△) and numerical (*) data in function wind speed values. 69

List of Tables

3.1 Main dimensions on the C-D model design (Paulo 2013). 37
3.2 Sizing Mesh details applied on generation grid for models blade. 38
3.3 Boundary Conditions. 39
3.4 Optimal angular speed that rotor generates. 45
3.5 Methods applied in spatial discretization solutions. 45

4.1 Drag and lift force values (N) obtained in the evaluation of aerodynamic blade model 1. 48
4.2 Drag force and lift force values (N) obtained in the evaluation of aerodynamic blade model 2. 49
4.3 Comparison of electric power production data in function of wind speed values obtained for both situations. 53
4.4 Comparison of power coefficient data in function of wind speed values obtained for both situations. 55
4.5 Computed wind turbine torque as a function of the wind speed values. . . 60
4.6 Comparison between experimental torque data attained with the numerical torque values in function of wind speed values. 69

Nomenclature

C-D	Concentrator-Diffuser
CAD	Computer-Aided Design
CFD	Computational Fluid Dynamics
DAWT	Diffuser Augmented Wind Turbine
DNS	Direct Numerical Simulations
HAWT	Horizontal Axis Wind Turbines
IGES	Initial Graphics Exchange Specification
MUSCL	Monotone Upstream-Centered Schemes for Conservation Laws
RANS	Reynolds-Averaged Navier-Stokes
SIMPLE	Semi-Implicit Method for Pressure-Linked Equations
SIMPLEC	Semi-Implicit Method for Pressure-Linked Equations Consistent
SRS	Scale-Resolving-Simulation
UWT	Urban Wind Turbines
WT	Wind Turbine

Chapter 1

Introduction

1.1 Motivation and Objectives

Large spread of wind technologies around the world has followed the constant increment on energy consumption. Urbanized areas are large consuming centers and where integration of designed Urban Wind Turbines, UWT, could be encouraged. Wind energy in urban environment shown some sustainable energy potential for exploitation.

Day by day electricity becomes a decisive factor on the growth of economics and sustainable development. Thus, associated with the increasing need for electrical power, synergies with best practices should be established for it's production. Linked to the decentralization of energy production, it became possible an approach of electric power producers elements with major consumption centers. Therefore, efforts to increase of energetic wind turbine performance should be made, and small wind turbines should be considered as part of the solution. These equipment's must accommodate increase in their energy performance, such that small energy gains, would contribute more to the sustainable development.

In this work, improvements on the energy production of small wind turbines (WT) were studied. These improvements were obtained placing the rotor inside a C-D, designed to accelerate the wind mass flow that pass through the rotor. Moreover, contributions on the experimental and numerical simulations were produced, in order to verify enhance that C-D produces in wind turbine production. C-D implementation verifies significant considerations that would become a designed aerodynamic device that hereafter, will be able to exploit the high potential exploitation present in the urbanized areas.

1.2 State of the Art

During the last years, significant progress has been made to understand the diffuser technology. Thus, new ideas have emerged on the origin of those technologies due to the

potential increase in efficiency that diffuser devices produce in wind turbines, particularly for small wind turbines.

Numerous investigations relative to Diffuser Augmented Wind Turbine, DAWT, or shrouded wind turbines concept over the last century were done.

As reported by Ten Hoopen (2009), Betz (1929) was the first to acknowledged the potential of ducted / diffuser wind turbines. The idea of DAWT in a preliminary study were proposed again by Lilley et al. (1956). The work from Lilley et al. (1956) the increase in axial velocity and reduction of blade tip losses was described as been as the main factors to enhance the power. A creation of a flow augmentation was also suggested, where laying of a flap at diffuser exit plane would raise the power augmentation.

As described by Phillips (2003), Lilley et al. (1956) regarded the cost of ducted windmill energy devices and suggested that one enhance of gain in power of at least 65 % relative to conventional wind turbines is achievable.

Analyzing different shrouded rotors, Kogan & Seginer (1963) concluded that the design is one of the main factors to obtain a power augmentation. Nevertheless, they suggested that the size of the duct become a commercially uncompetitive design. Furthermore, some serious flow separation inside the diffuser were described.

Experimental studies performed by Gilbert & Foreman (1983, 1979) and Igra (1981), shown that power extraction beyond Betz limit is possible. Furthermore, DAWT technology have been considered not profitable relatively to conventional wind turbines. Therefore, these investigations were not continued.

In the case of Igra (1981) work, the power enhanced of a shrouded wind turbine is described as been as a direct consequence of the sub-atmospheric pressure created around the rotor and at the exist plane of the diffuser. These sub-atmospheric pressures generate one effect of suction that produces a higher mass flow.

Several maximum power coefficient values were reported and different mechanisms that governing DAWT augmentation phenomena were proposed. The work from de Vries (1979) stated that DAWT power augmentation is ruled by the force that simple diffuser exerts on the flow. Furthermore, one analytical approach was made, based on work developed by Igra (1981), verifying in a maximum power coefficient of 0.7698.

Relative to renewed interest in DAWTs, an increasing number of publications have been released and several attempts has been made to commercialize the idea.

The DAWT design and performance was optimized by Phillips (2003), applying CFD methods, in which the wind turbine was modeled as an actuator disk. Also several small scale experiments were developed. Phillips (2003) concluded that the data of the full-scale DAWT shown only an augmentation of 2.4 instead of the expected 9, described in other publications.

Recently, according some authors, a shaped diffuser structure involving the wind turbine was applied. Furthermore, the structure includes a flange attached at the exit plane

of the diffuser.

Bet & Grassmann (2003) developed a shrouded wind turbine with a wing-profile ring structure. An increase in power output by the wing system of 2.0 was obtained. Additionally, Grassmann et al. (2003) continue the work performing some experimental measurements using a non-optimized wind turbine. The increase of power output in a factor of 55 % for high wind speeds and 100 % at low wind speed was described.

Wang et al. (2008) investigated convergent-divergent scoop effect on the power output applying on small wind turbine. Results shown that the scoop increases the airflow speed and enhance the power output 2.2 times relative to conventional wind turbines. These results also indicate that electricity yield can be improved at lower wind speeds.

On Ohya & Karasudani (2010) a remarkable increase, in the output power of approximately 4-5 times relative to conventional wind turbine is described. This, significant increment, is induced by the low-pressure region, that generates a zone of strong vortex formation behind the broad brim that draws more airflow to the wind turbine inside the diffuser.

Kosasih & Tondelli (2012) performed experimental studies of shrouded micro wind turbines. Experimental measurements of coefficient performance shown an increase of 60 % in addition of a simple conical diffuser, and 63 % with the addition of nozzle - conical diffuser shroud compared to the performance standard small wind turbines. Furthermore, it's described how the diffuser length and brim height can affect the performance augmentation of micro wind turbines.

As described in Jafari & Kosasih (2014) diffuser generates a sub-atmospheric region at downwind, which seems to attract more wind through the rotor relative to a conventional wind turbine. The work from Van Bussel (2007) showed that power augmentation is related to mass flow augmentation which is performed by increase of the exit area ratio and decrease of back pressure.

With modern computing power, more CFD studies have been performed on DAWT including blade and shroud design.

Applying numerical simulations and Particle-Image-Velocimetry in wind tunnel experiments Kardous et al. (2013) concluded that the utilization of a diffuser with a flange is responsible of a wind speed increase rate ranged from 64 % to 81 % while diffuser without flange is responsible only a increase rate of 68 %.

Toshimitsu et al. (2008) performed flow velocity measurements with flanged diffuser by Particle-Image-Velocimetry. Results shown that turbine blades rotating effects suppress the turbulence and the flow separation near the inner diffuser surface. At diffuser downstream some vortices, was consistently found such as, one behind the flange acts suction effect on wind to the diffuser, consequently raise the inlet flow velocity. Hence, diffuser device enhance the wind power in 2.6 times relative to standard wind turbine.

Aranake et al. (2013, 2014) performed some computational analysis of shrouded wind

turbine configurations, and a low ratio between shroud radius to shroud chord length of the diffuser is desirable, this indicate that the benefit of introducing shroud to a wind turbine is more easily to realize in small wind turbines, where this ratio is feasible. Likely verified in previous works, the shroud can be used effectively at low cut-in speeds and offers improve on the energy capture. Augmentation ratio of up to 1.9 with the introduction of a shroud was obtained.

According with Mansour & Meskinkhoda (2014), CFD calculation was performed, applying two different turbulence models for flow field around flanged diffuser. In short, a remarkable increase in wind speed of 1.6-2.1 times higher compared to small wind turbine was described. Furthermore, the turbulence models present the capability of providing reasonable predictions for complex turbulent flows.

As previously mentioned the use of a diffuser induces flow separation, nevertheless as seen in previous work flow separation can be suppressed. Extensive work from Gilbert & Foreman (1979) were made. The swirling flow produced by the rotor delays flow separation inside the diffuser was concluded due to a momentum transfer to the boundary layer.

Abe & Ohya (2004), Ohya & Karasudani (2010) have performed an extensive experimental and numerical work that lead to the development of one high performance flanged diffuser applied on small wind turbines. The pressure in the wake downstream of the diffuser adding a flange around the trailing edge of the diffuser, causing the flow to separate and create a large low pressure region downstream of the diffuser creating a suction effect through the diffuser was generated.

According with Shives & Crawford (2010) the flow separation of the boundary layer in diffuser sections leads to significant loses in performance of DAWT. Nevertheless, the base pressure effect provides a considerable enhancement.

Takahashi et al. (2012) worked on development of Wind-Lens turbine. The induced vortex formed, probably by blade tip vortex within the boundary layer of the inner surface of the diffuser, suppresses the flow separation from the inner diffuser surface. As result collection and acceleration of the wind is augmented.

Jafari & Kosasih (2014) reported that flow separation in diffuser may lead to reduces on overall power coefficient. This phenomenon can be mitigated by adapting the length of the diffuser.

A new version of the classic Betz limit has been proposed by Jamieson (2008), which describe that the maximum power extracted from a wind turbine with augmentation is 0.89 of the available power.

Recently, some methods to analyze the DAWT have been proposed. Vaz et al. (2014) proposed innovative 1D mathematical model approach to the analysis of DAWT using Blade Element Momentum model. Carroll (2014) creates one similar method to the way blade element momentum theory for a quick analysis tool for DAWT using an axisym-

metric surface vorticity method. It's clear that these preliminary studies need validation studies.

In short, DAWT configuration has received several evolutions on the understanding of the phenomena that governing the effect that enhances the wind turbine production with a shroud device. However, all of this knowledge acquired, not led to any commercial success so far by any company. Also, no commercial DAWT design tools have been developed so far and it seems that the scientific community still has to agree on the phenomena that govern the DAWT applications.

Concerning to this work, Enhanced Wind Turbine project has emerged from the work developed by Paulo (2013).

Main idea of *Enhanced WT* is enhance the productivity of urban wind turbines. Therefore, enhanced is achieved by encapsulating the wind turbine, accelerating the air flow and thus creating more electric energy. Previous work developed by Ribeiro et al. (2013) describe that *Enhanced WT* shows a yield 120 % higher than the small wind turbines conventional models.

Enhanced WT is composed by a convergent - diffuser and a wind turbine, as can be seen in following Figure.

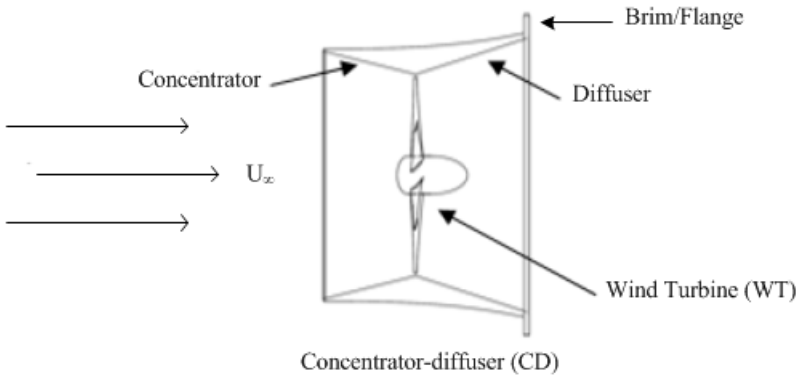

Figure 1.1: Schematic system representation composed by a concentrator-diffuser (C-D) and a wind turbine (WT), developed by Paulo (2013).

Also, at diffuser exit plane is accommodated a brim/flange, in order to exploit the suction effect.

Moreover, in the phase of creation of the encapsulated parts of the structure sustainable materials are used. Materials like cork base products are integrated in the equipment.

Due to the potential application in urban environments this equipment have a positive approach to urban space and the user. Moreover, initially enviable locations, low wind speeds or proximity of structures will become a favorable local to it's installation.

Associated with the project *Enhanced WT* some research activities has been developed. The work from Paulo (2013), experimental and numerical studies for development

and optimization of a shroud device for acceleration the wind to increase power in a wind turbine were performed. Through numerical simulations, one medium power increase of 71 % was obtained relative to standard wind turbine. Nevertheless, are verified higher values in the case of wind tunnel measurements. Therefore, the medium power increase of 107 % was obtained.

According with García-Abril (2014), numerical studies were performed for enhance the performance, optimizing the diffuser outlet angle. Despite of several angle have been studied, the 25º (without roughness) and 27º (with roughness) was considered those that enhance the power. These models suggest an improvement of 3.6 % to 8.7 % relative to a initial model (20º). As noted previously this study also concluded that the use of shrouded rotors induce a suction effect due to a pressure gradient generated in outlet of C-D.

Associated with the development and investigation of the research project *Enhanced WT* was created and tested a prototype, as can been seen from Figure 1.2. Presently, this project is in final prototype phase and soon pre-industrial series will accommodate some progress.

Figure 1.2: *Enhanced WT* prototype tested at 12 meters in unbuilt environment.

1.3 Structure

The fundamental motivations of this work are presented in Chapter 1, along a literature review on the shrouded wind turbines and a review of *Enhanced WT* project. In Chapter 2, the fundamentals concepts/theories of wind turbines aerodynamics are presented with the main theoretical concepts of Computational Fluid Dynamics (CFD). Chapter 3 is dedicated to presentation of the several methodologies applied on experimental and numerical tests. Chapter 4 includes a detailed analysis of the results obtained in the experiments and in numerical simulations. Finally, in Chapter 5, the main conclusions and suggestions for future work are described.

Chapter 2

Literature Review

Along this chapter, is presented the main theories for the assessment of shrouded wind turbines and for blade aerodynamics evaluation. Also are depicted several concepts related to the Computational Fluid Dynamics component.

2.1 Wind Turbine Aerodynamics

The existence of accurate models of aerodynamics aspects of wind turbines is one key point for a successful designing and analyzing wind energy systems. Wind turbines operation induces phenomena like cross-flow components (when a rotor is not aligned with wind), where magnitude and direction relative to the rotor changes as the blades rotate. Moreover, in these cases, phenomena like flow separation and three-dimensional effects becomes significantly more complex. Those instabilities interacting with blade, hub and tip form vortices that affect the character of the whole flow field. Clearly, wind turbine aerodynamics becomes more complex with all instabilities and flow interactions (Jonkman 2003).

Firstly, to understand the complex physics involving wind turbine aerodynamics, one should analyze a simple one-dimensional model.

The following sections were performed for an incompressible fluid. According with literature the flow velocity is a factor that determines the compressible or incompressible of the flow. Usually, as the blade tip speed do not exceeded 100 m/s which is equally to an Mach number of 0.3, and thus the flow around the rotor is assumed to be incompressible (Schlichting 1979).

2.1.1 Actuator Disc Model and Betz Limit

The simplest one-dimensional wind turbine model is so-called as actuator disc model where the turbine is replaced by a circular disc through which the flow streamlines passes with a velocity, U_∞.

The following equations presented in this section were based from Wilson & Lissaman (1974), Jonkman (2003), Manwell et al. (2002), Kulunk (2011).

The analysis assumes a control volume and are need to considers some assumptions: Wind is steady, homogeneous and have a fixed direction; air is incompressible, inviscid; an infinite number of blades need to be considered; a non rotating wake is considered; uniform thrust over the rotor needs to be assumed and the static pressure far upstream and far downstream of the rotor is equal to the undisturbed ambient.

A simple schematic of this control volume is shown in Figure 2.1.

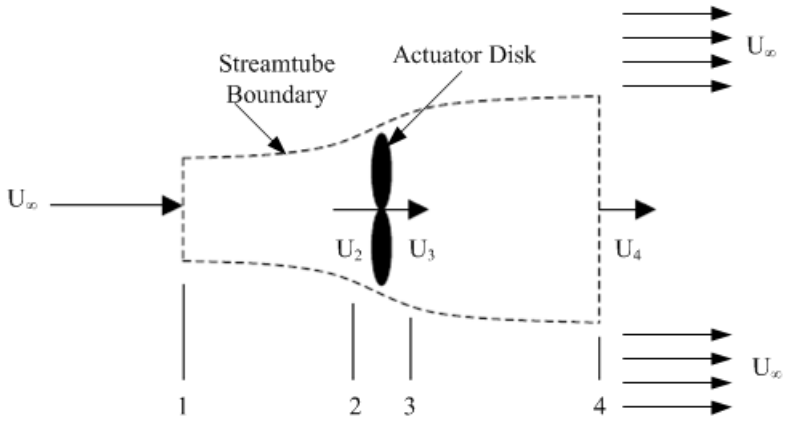

Figure 2.1: Actuator disk model of a wind turbine, adapted from (Jonkman 2003, Manwell et al. 2002).

In order to study this control volume, four regions (Figure 2.1) need to be considered as: 1: free-stream region; 2: before rotor; 3: after rotor and 4: far wake region. In free-stream region is assumed that $U_\infty = U_1$.

Applying the conservation of linear momentum to the control volume, and considering a steady-state flow, the thrust is equal to:

$$T = \dot{m}(U_1 - U_4) \tag{2.1}$$

where, $\dot{m}$ is the mass flow rate, and is equal to $\dot{m} = (\rho AU)_1 = (\rho AU)_4$, representing, ρ, air density, A the cross sectional area and, U, the air velocity.

The thrust is positive so the velocity behind the rotor, U_4, is lower than the U_1.

Since the flow is frictionless and there is no work or energy transfer is done, Bernoulli equation can be applied on both sides of the rotor.

$$p_1 + \frac{1}{2}\rho U_1^2 = p_2 + \frac{1}{2}\rho U_2^2 \tag{2.2}$$

$$p_3 + \frac{1}{2}\rho U_3^2 = p_4 + \frac{1}{2}\rho U_4^2 \tag{2.3}$$

where it's assumed that the far upstream and far downstream static pressures are equal

($p_1 = p_4$) and the velocity across the rotor stays equal ($U_2 = U_3$).

The thrust on the rotor disk, T, is also the differential pressure between stations 2 and 3 multiplied by the disc area:

$$T = A_2(p_2 - p_3) \tag{2.4}$$

Using Equations 2.2 and 2.3 and substitutes that into Equation 2.4 is obtained:

$$T = \frac{1}{2}\rho A_2(U_1^2 - U_4^2) \tag{2.5}$$

Recognizing now that $\dot{m} = A_2U_2$ and equating the thrust Equations 2.1 and 2.5, are obtained:

$$U_2 = \frac{U_1 + U_4}{2} \tag{2.6}$$

Thus, the wind velocity at rotor plane, is the average of the upstream and downstream wind speeds.

An axial induction (or interference) factor, a, measures the influence of the wind being slowed down as result of power extraction by the rotor. It's defined as the fractional decrease in wind velocity between the free stream and the rotor plane:

$$a = \frac{U_1 - U_2}{U_1} \tag{2.7}$$

$$U_2 = U_1(1 - a) \tag{2.8}$$

$$U_4 = U_1(1 - 2a) \tag{2.9}$$

The power extracted from the wind by the rotor, P, is the product of the thrust, T, and the wind velocity at the rotor plane, U_2.

$$P = TU_2 \tag{2.10}$$

$$P = \frac{1}{2}\rho A_2(U_1^2 - U_4^2)U_2 = \frac{1}{2}\rho A_2U_2(U_1 + U_4)(U_1 - U_4) \tag{2.11}$$

Substituting for U_2 and U_4 from Equations 2.8 and 2.9 gives:

$$P = \frac{1}{2}\rho AU^3 4a(1 - a)^2 \tag{2.12}$$

where the control volume, A_2, is replaced with A, the rotor area, and the free stream velocity U_1 is replaced by U.

Wind turbine rotor performance is usually characterized by it's power coefficient, C_P,

representing the fraction of available power in wind that is extracted by the turbine, is defined as:

$$C_P = \frac{P}{\frac{1}{2}\rho A U^3} \tag{2.13}$$

Substituting the extracted power form Equation 2.12 into Equation 2.13:

$$C_P = 4a(1-a)^2 \tag{2.14}$$

The theoretical maximum power coefficient from an idealized rotor, C_{Pmax}, known as Betz limit, can be found by setting the following derivative with respect to a equal to zero, and solving for a:

$$\frac{\partial C_P}{\partial a} = 4(1-3a^2) = 0 \rightleftarrows a = \frac{1}{3} \tag{2.15}$$

Substituting into Equation 2.14, yielding:

$$C_{Pmax} = \frac{16}{27} \approx 0.59259 \tag{2.16}$$

For an idealized wind turbine, the maximum efficiency is equal to 59.3 %. In practice, some considerations can be listed for real wind turbines do not present this efficiency: Rotation of the wake caused by the rotor; finite numbers of blades; viscid flow causes nonzero aerodynamics drag.

2.1.2 Effects of Wake Rotation on Betz Limit

Wakes behind Horizontal Axis Wind Turbines, HAWT, are a complex turbulent flow structures with rotational motion induced by the turbine blades movement, pressure slopes and tip vortices (Mo et al. 2013).

Two type of characteristics of wind turbine wakes can be enumerated: the velocity deficit, which is related to the power loss from wind turbine and turbulence levels, which may affect aerodynamic performance of other turbines located at downwind. Understanding these effects is among the main reason why turbines wakes have been subjected to a consistent research (Chamorro & Porté-Agel 2009).

Moreover, a clear analysis of these effects in consideration of Betz limit proves to be an important consideration for the study of aerodynamic performance of HAWT.

The previous analysis can be extended to the case with rotating rotor generates angular momentum, having relationship with rotor torque. The flow behind rotor have an opposite rotation direction relative to wind turbine rotor. Present reaction is caused by the torque exerted by the flow on the rotor. Figure 2.2 shows an example wake rotation generated by a wind turbine.

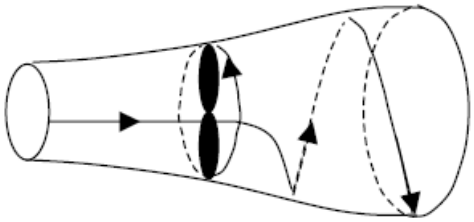

Figure 2.2: Wake rotation structure (Jonkman 2003).

The generation of rotational kinetic energy in the wake produces a lower energy extraction by the rotor that would be expected without wake rotation. Thus, with increasing of torque generation therefore will be also verified a higher production of the kinetic energy in the wind turbine wake.

Following a procedure similar to that used in section 2.1.1, accounting with wake rotation those equations can be used to modify the theoretical maximum power coefficient for an idealized rotor, C_{Pmax}. According with the work developed by Eggleston & Stoddard (1987), values of theoretical maximum power coefficient where obtained considering the wake rotation phenomena.

It's worth noticing that, the work developed by Eggleston & Stoddard (1987) evaluates the maximum power coefficient as function of the tip speed ratio. The tip speed ratio, λ, is defined as the ratio of the blade tip speed to the free stream wind speed and is calculated as:

$$\lambda = \frac{\Omega R}{U_\infty} \tag{2.17}$$

where, Ω, is angular velocity and, R, is the radius of turbine blades.

Thus in following Figure 2.3 those values are comparable with the Betz limit.

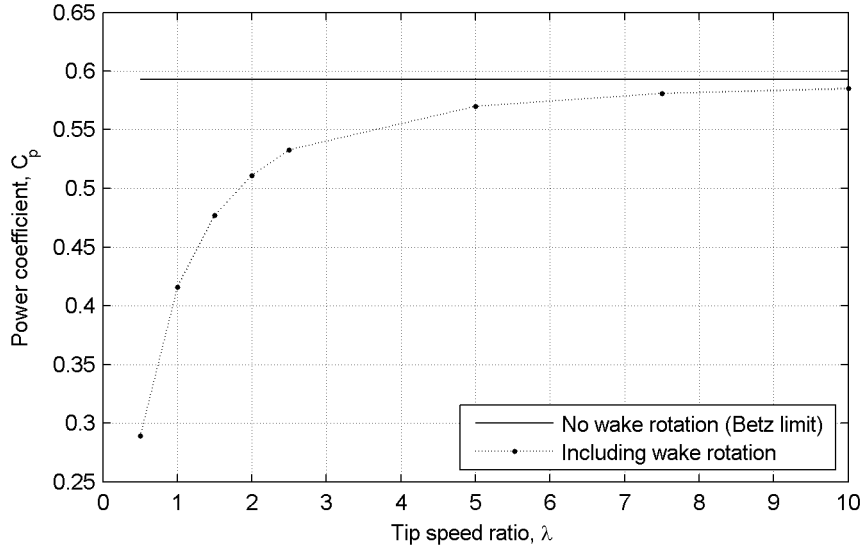

Figure 2.3: Theoretical maximum power coefficient as function of tip speed ratio for an ideal HAWT, with and without wake rotation, adapted from Eggleston & Stoddard (1987).

Extending this analysis to different wind turbine types an identical evaluation of power coefficient as function of tip speed ratio can be performed. Thus, in following Figure 2.4 is described that evaluation.

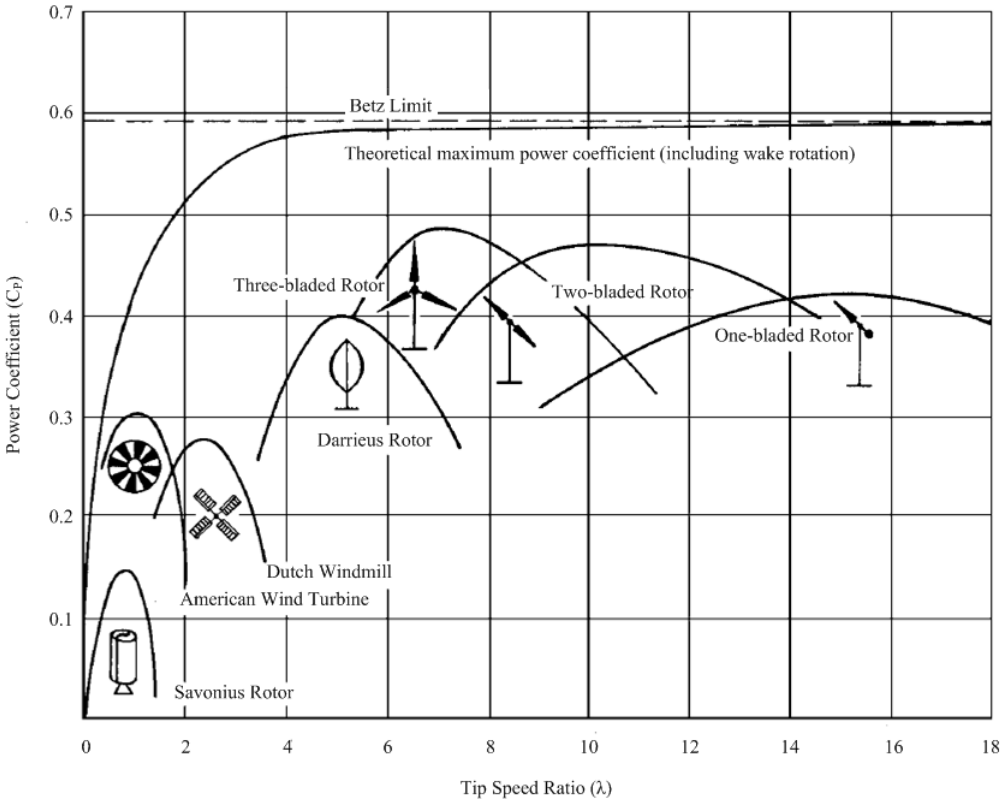

Figure 2.4: Theoretical power coefficients (C_P) of wind rotors considering different designs as function of tip speed ratio (λ) (Wilson & Lissaman 1974, Hau 2006).

In Figure 2.4 are presented power coefficients performances of rotors that presents different configurations. Nevertheless, is emphasized the performance curve of American Wind Turbine, due to this configuration be considered similar to the studied in this work. From all the configurations described in Figure 2.4, it appears that the American Wind Turbine, describing 8 blades, displays a configuration closest to the used in this work, which features 6 blades.

2.1.3 Theoretical Analysis of Shrouded Rotor

In order to evaluate concepts like shrouded rotors is prudent to examine the theoretical background which governing performance of shrouded rotors.

According with augmentation ratio, r_a, is possible to describe the enhance power extracted from a wind turbine combined with a diffuser. Therefore, augmentation ratio is defined as (Aranake et al. 2013):

$$r_a = \frac{C_{P,d}}{0.593} \tag{2.18}$$

where $C_{P,d}$ is power coefficient for a wind turbine with diffuser.

Shrouded rotors can combine different systems in order to help to concentrate and accelerate the wind. Hollow structures can be applied for surrounding a wind turbine to enhance the wind flow. As can been seen in Figure 2.5 nozzle model section reduces the inside cross-section, in cylindrical model section may have a constant cross-section, and diffuser model section have cross-section at downstream that expands (Ohya et al. 2008).

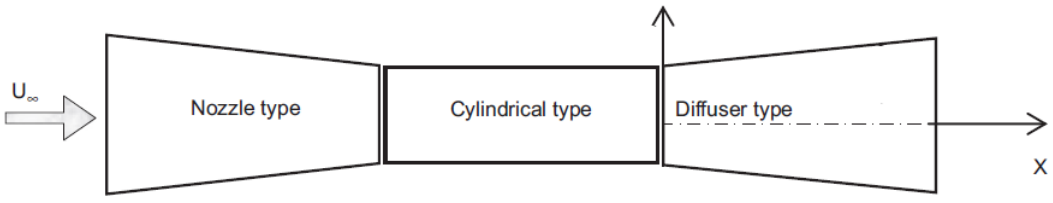

Figure 2.5: Schematic representation of systems that concentrate and accelerate the wind, adapted from Ohya et al. (2008).

Applying nozzle, with converging shape, at inlet of shrouded wind turbine, will become beneficial mainly in variable wind direction flow condition, which is typical in urban scenario (Kosasih & Tondelli 2012).

The shrouded rotors exploit the Venturi effect, where the reduction of fluid pressure and the associated elevation of fluid velocity, are produced by the passage of a flow in a contraction. For a shrouded rotor, the contraction is performed by the shroud that surrounding the rotor (Hjort & Larsen 2014). At nozzle section, the inlet diameter is larger than the outlet diameter, due to this the air velocity at the inlet is lower. Moreover, when

it comes to the outlet, the velocity gets increased due to the reduction of area (Balaji & Gnanambal 2014).

The principle of increase the mass flow through the wind turbine can be combined with the turbulent mixing of the wake behind the rotor providing a power augmentation (Ten Hoopen 2009).

It's well proven that when a bare wind turbine is operating at the maximum Betz limit, the airflow is decelerated to $2/3$ of the free stream velocity. This flow deceleration causes a pressure increase in front of the rotor that induces a small portion of the mass flow being pushed sideways around the rotor (Ten Hoopen 2009).

A mechanism to increase air flow can be applied placing an annular lifting device around the rotor. This device is known as a shroud or a diffuser of annular wing. The increase in diffuser exit plane velocities combined with a reduction of static exit pressure and consequently is obtained an enhanced of mass flow leading to a higher extraction of energy potential. The principle behind a DAWT can be assumed as the cause of the air flow on the inside the diffuser to accelerate. Furthermore, the suction is related to the lift of the airfoil and according to the Kutta Joukowski theorem, related to the bound vorticity. The annular airfoil generates a radial lift force creating a ring vortex, based on Bio-Savart law, that consequently will induce a higher velocity on the suction side. Furthermore, this higher velocity enhance the mass flow through the rotor plane (Ten Hoopen 2009).

Associated at energy extraction from an air flow a wake behind the rotor is produced. This wake has a pressure and a velocity deficit relative to undisturbed free stream flow. According with (Igra 1981, Van Bussel 2007), the power augmentation of a DAWT is a direct consequence of the sub-atmospheric pressure around the rotor and exit plane of the shroud.

DAWT configuration allows tip vortices created at the blade tips to be significantly less due to close proximity of the diffuser wall. Therefore, mixing potential behind the exit plane of a DAWT is expected to be higher than in the case of conventional wind turbine (Ten Hoopen 2009).

The mixing of effect on diffuser leeward provides one wake flow with more volume. Furthermore, a larger wake volume will induce lower exit pressures behind the rotor and therefore more suction effects (Ten Hoopen 2009).

In order to take advantage of mixing effects flanged applications on shroud plays an important role. This flanged, also known as brim, collects and accelerates the approaching wind (Ohya et al. 2008). The flanged is placed at the exit plane of the shroud, such as in Figure 2.6, and mimics the Guerney flap used in F1 racing cars (García-Abril 2014)

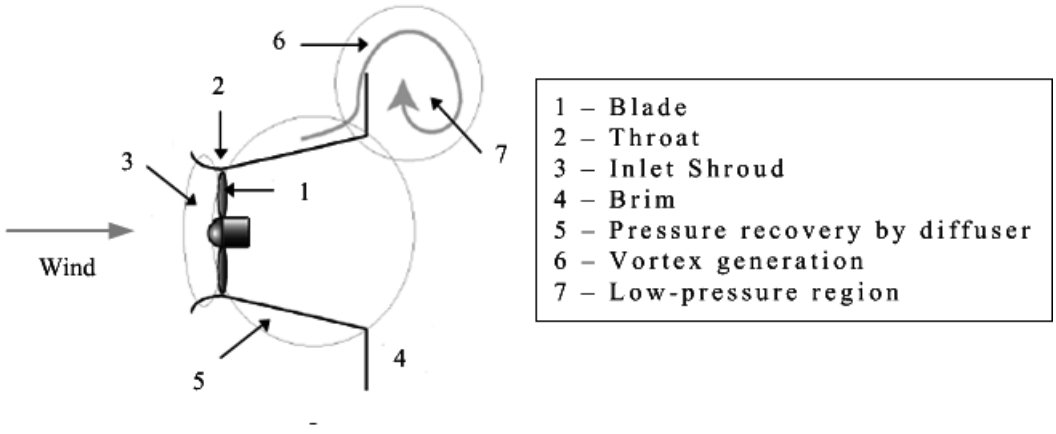

Figure 2.6: Representative illustration of the flow around the shroud, considering the presence of brim, adapted from Ohya & Karasudani (2010).

The flange is a structure ring-type plane with a variable height may affect the shroud performance. It's placed attached vertically to the outer periphery of exit shroud (Ohya et al. 2008, Kosasih & Tondelli 2012).

As can be seen from Figure 2.6, the flange induces a low-pressure region in the near wake of the diffuser by vortex generation. Furthermore, more mass flow is drawn to the inside of shroud (Ohya et al. 2008, Ohya & Karasudani 2010, Takahashi et al. 2012). The flange causes vortices formation, an enhancer in the pressure drop and, consequently, an increase the air speed of the outlet. An increase the air velocity in the diffuser, is therefore, achieved (Mansour & Meskinkhoda 2014).

In Figure 2.6, the "throat" plane represent the diffuser cross section perpendicular to the axisymmetric axis where the area inside the diffuser is smallest (Hjort & Larsen 2014).

An important characteristic can be described from the application on a brimmed diffuser shroud. Brim application helps the shroud, for automatically, stay aligned to the approaching wind. Another characteristic verified at low-tip speed ratio range that vortex generated from blade tip becomes suppressed through the interference with the boundary layer within the diffuser shroud. Therefore, aerodynamic noise is substantially reduced (Abe et al. 2006, Ohya & Karasudani 2010).

2.1.4 Forces Acting on a Blades

Mainly can be shown two examples of manifestation the main forces in wind turbine operation. Expression of drag force can be evidenced when a wind turbine presence high wind and is stationary where the primary consideration is the drag force. In contrast, when a wind turbine is operating it's lift force, produced by blades, which create aerodynamic loading and consequently is generated mechanical energy (Burton et al. 2001, Manwell et al. 2002).

At fluid mechanics principles, when occurs a flow around asymmetric object, the flow

field downstream of the object will be asymmetric and the velocity and pressure downstream and upstream will be different. Consequently a normal force to flow will generated in object. The same behavior is verified for objects whose axis isn't perfectly aligned. Therefore, is expected that the action of friction tension will produce a resultant force pair in opposite direction of flow due to boundary layers of surface body. Thus, this force is opposed to motion of body (Vennard et al. 1996).

In short, the pressures and friction tensions produce a resultant force pair perpendicular between themselves designed by drag and lift. Therefore, the drag produced by flow around an object is defined as the forces that act on body in the parallel direction to flow direction. Relatively to lift is defined like a force that act on body in a normal direction to flow direction (Burton et al. 2001, Vennard et al. 1996). These characteristics are depicted in following Figure 2.7.

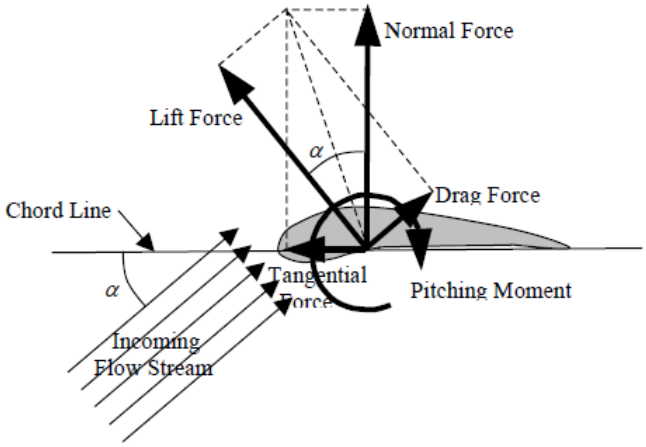

Figure 2.7: Resultant forces acting on an airfoil (Jonkman 2003).

An effective moment results of these forces. Thus, usually is defined about on normal axis to the cross-section of the airfoil, located at quarter of the distance from the leading edge to the trailing edge (Jonkman 2003).

The forces acting on an object by a flow are due to pressure and viscous stresses. On the upper surface of an airfoil, the pressure is less than that of the flow stream which sucks the airfoil upward, normal to the incoming flow. On the other hand, the pressure on the lower surface of the airfoil is greater than that of the flow stream and effectively pushes the airfoil upward. Due to this, pressure distribution component tends to slow the velocity of the incoming flow relative to the airfoil, as well as viscous stresses (Jonkman 2003). Moreover, typical pressure distribution around an airfoil is shown in Figure 2.8.

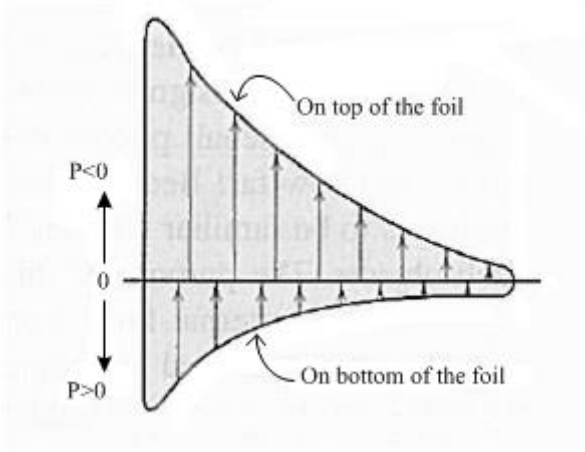

Figure 2.8: Pressure distribution around an airfoil (Vennard et al. 1996).

The pressure distribution of both sides of the airfoil, present on Figure 2.8, have a positive contributions to lift generation. By contrast, the viscous stresses have a negligible contribution to the lift force. The part of the drag force related to pressure distribution around the airfoil is classified as pressure drag. Thus, the part relative to viscous stresses is known as skin-friction drag. Sum of both perform total drag force, defined as drag (Jonkman 2003).

The drag force, F_D, and lift force, F_L, are defined respectively as:

$$F_D = \frac{1}{2} \times \rho \times C_D \times A \times U_\infty^2 \tag{2.19}$$

$$F_L = \frac{1}{2} \times \rho \times C_L \times A \times U_\infty^2 \tag{2.20}$$

where C_L and C_D are lift coefficient and drag coefficient, respectively and, A, represents blade area.

2.1.5 Airfoils

Airfoils, presents a well-designed form projected for integration on many areas such as wind blades conception (Chen 2011). Some terms usually are used for characterization of this structure, which are represent on Figure 2.9.

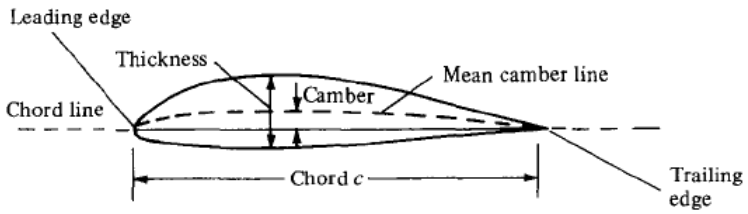

Figure 2.9: Airfoil nomenclature (Anderson 2001).

An airfoil, presents divided by the mean chamber line, which define the locus of points halfway between lower and upper surface. In most forward and rear points of this line are contained the leading and trailing edge, respectively. The line how connect leading and trailing edge is classified as chord line, and that distance measured in this line is designated as chord, c. The thickness is measured perpendicular to chord line, and is the distance among lower and upper surface. The chamber is represented as the distance between chamber line and chord line, also valued perpendicular to chord line (Manwell et al. 2002). At last, attack angle, α, if defined as the angle form between chord line and the relative flow.

In conception of wind turbine blades are regarded different shapes of airfoil along the cross-section of the blade. Along the length are verified different values of thickness. Thus, the blade tip is designed using a thin airfoil, for obtain a high lift to drag ratio. By contrast, root region is designed using a thick version of one airfoil to obtain strength important for structural support (Manwell et al. 2002).

2.1.6 Blade Element Theory

Blade element theory refers to an analysis of forces at a section of the blade, as a function of blade geometry. Following Figure 2.10 describes the blade divisions into dr section.

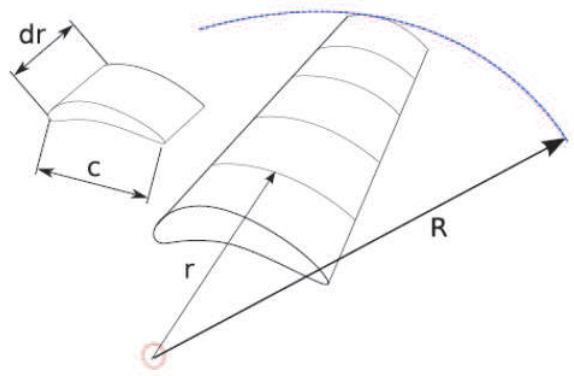

Figure 2.10: Blade element model, divided into dr section (Kulunk 2011).

Additional equations concerning the state of flow need to be developed. The state of flow governed by characteristics of rotor blades needs to use the blade geometry properties to determine the forces exerted on a wind turbine by the flow stream. This type of analysis is referred to as Blade Element Theory.

At each section blade and flow stream properties can be assumed differential rotor thrust, dT, and differential rotor torque, dQ. For this consideration certain assumptions needs to be made (Manwell et al. 2002):

- Between sections are not verified aerodynamic interactions;

- The forces that acts on the blades are set exclusively by the drag and lift characteristics of the airfoil shape.

The differential rotor thrust, dT, and differential rotor torque, dQ, acting on each blade section as described by blade element theory is represented on Figure 2.11.

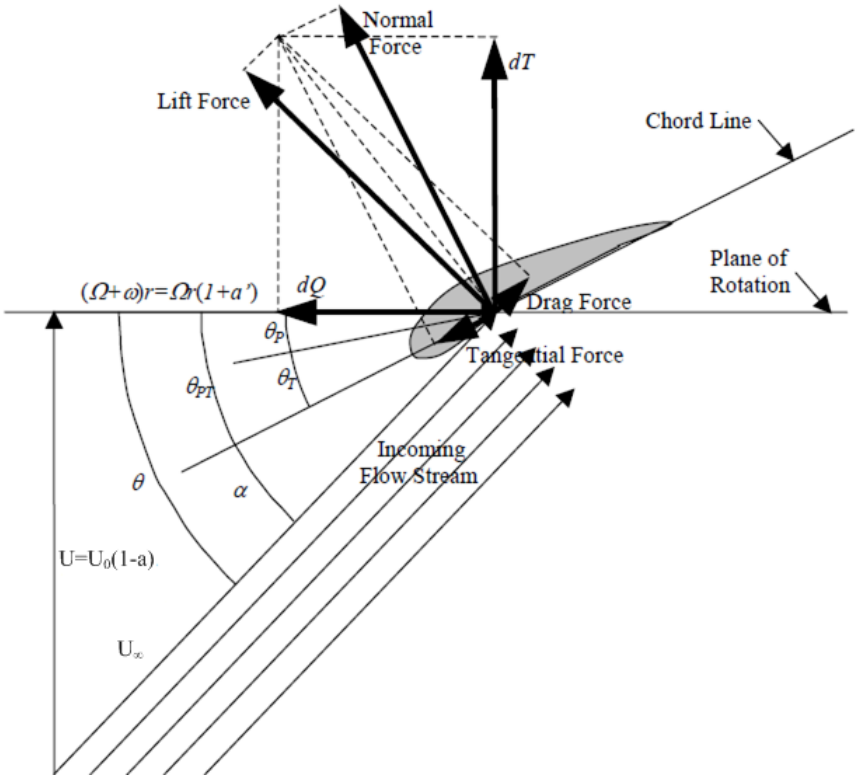

Figure 2.11: Blade geometry (cross section) for analysis of blade element theory (Jonkman 2003).

were, θ_P is the blade collective pitch angle measured relative to the point of zero twist, θ_T is the local blade twist angle and θ_{PT} is their sum.

Note also, that angle θ is the angle of the relative incoming flow stream with respect to the plane of rotation and is equal to the sum of θ_{PT} and α (Jonkman 2003).

The velocity of the incoming flow relative to the blade element geometry, U_∞, is the vector sum of the axial inflow velocity at the rotor plane, U, the inflow velocity caused by the rotation of the blade, Ωr, and the inflow velocity caused by wake rotation at the rotor plane, ωr (Jonkman 2003).

$$U = U_0(1-a) \tag{2.21}$$

$$\omega = \Omega a' \tag{2.22}$$

Through, blade geometry, U_∞, can be described as:

$$U_\infty = \sqrt{[U_0(1-a)]^2 + [\Omega r(1+a')]^2} \tag{2.23}$$

Also relation between a, a', and θ can be developed:

$$\tan(\theta) = \frac{U_0(1-a)}{\Omega r(1+a')} \tag{2.24}$$

Regarding the resultant forces some relationships can be extracted from Figure 2.11 (Jonkman 2003, Manwell et al. 2002):

$$F_L = \frac{1}{2} C_L \rho U_\infty^2 c dr \tag{2.25}$$

$$F_D = \frac{1}{2} C_D \rho U_\infty^2 c dr \tag{2.26}$$

where, c, represents chord dimension.

$$dT = F_L \times \cos(\theta) + F_D \times \sin(\theta) \tag{2.27}$$

$$dQ = r[F_L \times \sin(\theta) - F_D \times \cos(\theta)] \tag{2.28}$$

If the rotor has B blades, the differential rotor thrust, dT, and differential rotor torque, dQ are to following:

$$dT = \frac{1}{2} B \rho U_\infty^2 [C_L \cos(\theta) + C_D \sin(\theta)] c dr \tag{2.29}$$

$$dQ = \frac{1}{2} B \rho U_\infty^2 [C_L \sin(\theta) - C_D \cos(\theta)] c r dr \tag{2.30}$$

dT and dQ represents the total differential thrust and differential torque, respectively, acting on an annular ring of radius r and thickness dr. It's worth noticing, that the effect of drag force is to decrease torque and hence power, but to increase the thrust loading (Manwell et al. 2002).

Momentum theory uses a control volume analysis to study the forces at the blade based on the conservation of linear and angular momentum. Blade element theory refers to an analysis of forces at a section of the blade. The results of these theories can be combined and form a theory designed as blade element momentum (BEM) theory.

2.2 Numerical Simulation (CFD)

Wind turbine design and aerodynamic performance are an important scientific field. In this area, many researchers have developed numerical codes to support aerodynamic op-

timization to perform an upgrade on energy production of wind turbine (Lanzafame et al. 2013).

Computational fluid dynamics consists of solving the Navier-Stokes equations with governing fluid flow using approximation with numerical means (Sumner et al. 2010). CFD solvers are based on following three fundamental conservations principles expressed in terms of mathematical equations: Conservations mass; conservation of momentum and conservation of energy (Sargsyan 2010).

In Versteeg & Malalasekera (2007) is described that one of the fundamental task of the CFD user have is to design a grid that presents a suitable compromise between desired accuracy and solution cost. Another concerning in the numerical simulations simultaneously are moving and stationary components that exist, which must be handled separately (Bazilevs et al. 2011).

Extensive implementation of numerical simulations in aerodynamic features, applied on different manners, ranging from Blade Element Momentum methods integrated by CFD solver to full 3D Navier-Stokes models became an important manner to evaluate wind turbines performance (Sargsyan 2010).

Performing CFD calculations provide endless details knowledge of the fluid flow, such as velocities, pressure, temperature, turbulence, etc. Further, several type graphics are possible to obtain, performing results in flow lines, contour lines and iso-lines, etc. At this stage, is assumed by Castelli et al. (2013) that these results can be compared to that obtained in a wind-tunnel study or an elaborate full-scale measurement campaign.

3D CFD numerical codes are physically realistic, due to solve the Navier-Stokes equations. Nevertheless, to achieve these solutions longer computational times are needed. Also an accurate preparation of geometry is necessary. In spite of some problematic issues that involves separated flow modeling globally CFD codes are an important mean to achieve knowledge that are impossible to reach in experimental measurements (Lanzafame et al. 2013).

2.2.1 Governing Equations

The fluid dynamics involves complex relationships between the viscosity and how the flow develops, translating into mathematical models induces a high level of complexity for some problems (Massey 1996).

The true fluid flow passing through and around a wind turbine is governed by the main-principles of Navier-Stokes equations. Unfortunately, these equations are so complex that analytical solutions only have been found for simple cases. Although numerical solutions presents abilities to solve these equations (Jonkman 2003).

As shown by Trias & Lehmkuhl (2011) the incompressible Navier-Stokes equations form an excellent mathematical model of turbulent flows. The Navier-Stokes equations

are a set of partial differential equations that translate to a unit volume of fluid flow, a balance between the product of it's mass and the corresponding acceleration (Oliveira & Lopes 2012).

Major CFD models are based on the incompressible Reynolds-Averaged Navier-Stokes (RANS) equations derived from the main principles of conservation of mass and momentum Sumner et al. (2010):

$$\nabla \overrightarrow{U} = 0 \tag{2.31}$$

$$\frac{\partial \overrightarrow{U}}{\partial t} + \nabla \overrightarrow{U} = -\frac{1}{\rho}\nabla_p + \nabla\tau + \overrightarrow{f} \tag{2.32}$$

where, $\overrightarrow{U}$ represents the mean velocity vector, p is the modified mean pressure, ρ is the fluid density, $\overrightarrow{f}$ represents a body force and τ perform the specific Reynolds stress tensor.

2.2.2 Structure of CFD Code

CFD codes are constructed around numerical algorithms that are developed for resolution of fluid flow problems. Aiming to provide intuitive tools for users of complex CFD codes, normally these are divided in three elements: (i) Pre-processor, (ii) Solver, (iii) Post-processor (Versteeg & Malalasekera 2007).

The pre-processor phase consists in the introduction of physical flow model with the intention of converting in a mathematical model (Sargsyan 2010). The principles activities of user's are: definition of computational domain; grid generation of problem; modeling of physical/chemical phenomena (e.g. turbulence models, radiative heat transfer, combustion models); definition and specification of fluid properties and boundary conditions of cells which have relation with another boundary (Versteeg & Malalasekera 2007).

In general, the precision of solution obtained are governed by the number of cells in the grid. So larger the number of cells contained in grid domain, more accurate will be the solution. In short, both precision of solution as the cost in terms of computer capacity and calculation time are dependent on the grid excellence (Versteeg & Malalasekera 2007).

The principal element of CFD code is the solver. The core of CFD code works with discretization of governing equations fluid flows. In this phase, are modeled the unknowns and solved with a resolution of algebraic system of equations (Versteeg & Malalasekera 2007, Sargsyan 2010).

At last, post-processor phase analysis solution results. With the evolution of CFD packages results in a number of ways of visualization of solver outputs. So it's possible set graphs and contours, perform domain and grid visualizations, introduce vectorial plots and path-lines, and to perform also dynamic representations using animations (Sargsyan 2010).

2.2.3 Grid Generation

In numerical simulation applied for areas as science and engineering a mesh generation is often described being a fundamental pre-requisite. The growing of mesh generation brought new ideas and ways of viewing mesh related issues (Baker 2005).

It's well known that, approximately over 50 % of time spent in development of CFD projects is devoted to the definition of computational domain and grid generation (Versteeg & Malalasekera 2007).

Furthermore, a compromise between number of cells/domain size and computational time need to exist. Due to a consideration of one small domain would not provide enough grid generation, while a too great domain would lead to an increasing of computational time, that are unnecessary for certain cases (Lanzafame et al. 2013).

According to Baker (2005) grid generation has evolved to a point where complicated domains can be covered by a variety of mesh types.

Several grid types can be classified as structured, unstructured and hybrid type. In short, structured grids are defined by their regular connectivity, that is not verified in unstructured grids that presents an irregular connectivity between elements. Relatively to hybrid grids, these type contain an efficient mixture of structured portions and unstructured portions (Baker 2005, Bern & Plassmann 2000).

A major applications of unstructured grid is verified in finite elements calculations (Digraskar 2010).

The element quality and how this affect the solution accuracy is still a research area that has some question unanswered (Baker 2005). As like as "mesh quality" definition, that according to Knupp (2007) is defined as been as "the characteristics of a mesh that permit a particular numerical partial differential equation simulation to be efficiently performed with fidelity to the underlying physics and with the accuracy required for the problem". Associated to meshes composed by complex geometries two fundamentals issues can be described for the quality of a finite element mesh (Burkhart et al. 2013). The first can be considered as the shape of the elements that are selected to generate the mesh. Moreover, two element shapes (tetrahedral and hexahedral) for discretize the complex geometries are used. On the other hand, the coarseness of the mesh is also considered. In other form, the number of elements that the mesh is composed. Thus, in literature can be found that an optimal mesh density exists when is provided the most accurate solution with the smallest number of elements (Burkhart et al. 2013).

2.2.4 Finite-Volume Method

Most of the commercial CFD codes are based on the method of a finite volume discretization (Carcangiu 2008). The finite-volume method is responsible for sub divide the domain into a finite number of continuous control volumes, and thus the conservation equations

are applied to those control volumes (Ferziger & Peric 2002). This method can accommodate any type of grid, so it's suitable for complex geometries (Ferziger & Peric 2002). A detailed description of the finite-volume method is presented in Ferziger & Peric (2002).

FLUENT uses a cell-centered finite-volume method based on multidimensional linear reconstruction scheme. Allowing the use of computational elements with arbitrary polyhedral topology (quadrilateral, hexahedral, triangular, tetrahedral, pyramidal, prismatic) (Mo et al. 2013). FLUENT also uses a control-volume-based technique to remodel the governing flow equations into algebraic equations that can be solved numerically (Makridis & Chick 2013). This technique consists of integrating transport equation in each volume, resulting in a discrete equation that expresses conservation laws based on the logic of a closed control volume (Fleck 2012).

In short, control-volume technique used by FLUENT consists in: Division the domain into discrete control volume using a computational mesh; integration of the basic governing equation on the control volumes to produce algebraic equations for the discrete variables and application of linearization of the discretized equations and solution of the resultant equation system (Carcangiu 2008, Versteeg & Malalasekera 2007, Fluent 2011*a*).

In ANSYS FLUENT core are available two numerical methods, applied for several conditions. Pressure-based solver were developed for low-speed incompressible flows. Although, the second solver, designed as density-based solver, were created for application in high-speed compressive flows. In present work, involves incompressible flows clearly pressure-based approach was applied.

The pressure-based solver uses an algorithm that pertains to a group of methods designed as projection method. In this method, the restriction of mass conservation of the velocity field is achieved by solving a pressure equation. The pressure equation is derived from the continuity and momentum equation in such a way that velocity field, corrected by the pressure satisfies the continuity equation. The complete solution process involves iterations wherein the entire groups of governing equations are solved repeatedly until the solution converges (Fluent 2011*b*).

2.2.5 Turbulence Modeling

As previously stated in subsection 2.2.2, modulation of physical phenomena is one of the main issues that the user must take into account. Moreover, in this work will be taken into account the turbulence generated in problems of the fluid mechanics area. Therefore, to understand the turbulence modulation it's important firstly, to describe the Reynolds number.

Reynolds number, *Re*, is the ratio between inertia terms and viscosity in the Navier-Stokes Equations (Reynolds 1883, Stokes 1851).

$$Re = \frac{L \times U}{\nu} \tag{2.33}$$

where, L is the characteristic over a body dimension of the flow (m); U is the mean velocity (m/s); and ν is the kinematic viscosity (m^2/s).

The Navier-Stokes equations applied for model of turbulent flows, in some situations are impractical to resolve for some ranges of scales in Direct Numerical Simulations (DNS) due to high requirements of computing power. Therefore, averaging procedures need to be applied to Navier-Stokes equations to filter part of the turbulent spectrum. The principal averaging procedure applied is Reynolds-averaging of the equations, which result in the Reynolds-Averaged Navier-Stokes (RANS) equations. In this procedure turbulent structures are eliminated and it's feasible to obtain a smooth variation of the averaged velocity and pressure fields. However, RANS equations introduce additional unknown terms into transport equations which are solved by turbulence model (Fluent 2011*a*).

An alternative to RANS equations are Scale-Resolving-Simulation (SRS). In these methods, at least one section of the turbulent spectrum is solved in at least a part of the flow domain. Comparative to RANS simulations, all SRS methods require time-resolved simulations with small time steps. These methods also are considerably more computationally expensive than RANS models (Fluent 2011*a*,*b*).

RANS models are the most economic approach for computing of complex turbulence applications. Positively, RANS models are available for all range of applications providing a level of accuracy required. The most well-known models are k -ε and k - ω. These models contribute for simplify of the problem, adding two additional transport equations and introduce a turbulent viscosity to solve the Reynolds Stresses (Fluent 2011*a*,*b*, 2005).

The choice of turbulence model it's an important step to make once affect all quality of the simulations. For selection of turbulence model is necessary apply some considerations such as, fluid behavior, the level of accuracy required, the available computational resources, the time of simulation and provides a suitable numerical grid and the time spent (Fluent 2011*a*).

2.2.5.1 k - ε Model

By definition, two equation models include two extra transport equations for represent turbulent properties of the flow. For the case of k-ε models the first transported variable is often turbulent kinetic energy, k, which define the energy present in turbulent flow. The second transported variable is turbulent dissipation, ε, and represent scale of turbulence (*CFD-Wiki* 2005).

Two-equation models are the most widely used turbulent models in the CFD history. The main features of $k-\varepsilon$ models are robustness, the economic submitted in computer terms, and the behavior presented for wide range of turbulent flows generating a reason-

able accuracy (Fluent 2011*a*).

The standard form of the k - ε turbulence model is originally proposed by Launder & Spalding (1972) . Thus, following equations are described in *CFD-Wiki* (2005), Fluent (2005), Wilcox (1994). The turbulent kinetic energy, k, and it's dissipation rate, ε, are obtained from the following transport equations:

$$\frac{\partial}{\partial t}(\rho k)+\frac{\partial k}{\partial x_i}(\rho k u_i)=\frac{\partial}{\partial x_j}\left[(\mu+\frac{\mu_t}{\sigma_k})\frac{\partial k}{\partial x_j}\right]+G_k+G_b-\rho\varepsilon+S_k \tag{2.34}$$

$$\frac{\partial}{\partial t}(\rho\varepsilon)+\frac{\partial}{\partial x_i}(\rho\varepsilon u_i)=\frac{\partial}{\partial x_j}\left[\left(\mu+\frac{\mu_t}{\sigma_\varepsilon}\right)\frac{\partial\varepsilon}{\partial x_j}\right]+C_{1\varepsilon}\frac{\varepsilon}{k}(G_k+C_{3\varepsilon}G_b)-C_{2\varepsilon}\rho\frac{\varepsilon^2}{k}+S_\varepsilon \tag{2.35}$$

In these equations, G_k, represents the generation of turbulence kinetic energy due to the mean velocity gradients, and is described in Fluent (2005). G_b is the generation o turbulence kinetic energy due to buoyancy, calculated in Fluent (2005). $C_{1\varepsilon}$, $C_{2\varepsilon}$ and $C_{3\varepsilon}$ are constants, also σ_k and σ_ε are turbulent Prandtl numbers for k and ε. S_k and S_ε are user-defined sources terms.

The turbulent/eddy viscosity $(kg\,m^{-1}s^{-1})$ is modeled as:

$$\mu_t=\rho C_\mu\frac{k^2}{\varepsilon} \tag{2.36}$$

where the closure coefficients for standard $k-\varepsilon$ model are:

$$C_{1\varepsilon}=1.44,\ C_{2\varepsilon}=1.92,\ C_{3\varepsilon}=-0.33\ C_\mu=0.09,\ \sigma_k=1.0,\ \sigma_\varepsilon=1.3 \tag{2.37}$$

The use of Realizable $k-\varepsilon$ models is recommended relative to other variants of this family models, combining with Enhanced Wall Treatment (Fluent 2011*a*).

The realizable $k-\varepsilon$ model proposed by Shih et al. (1995) differs from standard model in two important ways: The realizable $k-\varepsilon$ model contains a new formulation for the turbulent viscosity; and a new transport equation for the dissipation rate, ε, is proposed. New transport equation have been reached from derivation of an equation transport of mean-square vorticity fluctuation. The terms "realizable" means that model satisfies "certain mathematical" constraints on the Reynolds stresses (Fluent 2005).

Note that following set of equations are described in Fluent (2005), Shih et al. (1995), Cabezón et al. (2011).

The modeled transport equations for the, k and ε, in the realizable $k-\varepsilon$ model are:

$$\frac{\partial}{\partial t}(\rho k)+\frac{\partial k}{\partial x_j}(\rho k u_j)=\frac{\partial}{\partial x_j}\left[(\mu+\frac{\mu_t}{\sigma_k})\frac{\partial k}{\partial x_j}\right]+G_k+G_b-\rho\varepsilon+S_k \tag{2.38}$$

$$\frac{\partial}{\partial t}(\rho\varepsilon)+\frac{\partial}{\partial x_j}(\rho\varepsilon u_j)=\frac{\partial}{\partial x_j}\left[\left(\mu+\frac{\mu_t}{\sigma_\varepsilon}\right)\frac{\partial\varepsilon}{\partial x_j}\right]+\rho C_1 S_\varepsilon-\rho C_2\frac{\varepsilon^2}{k+\sqrt{\nu\varepsilon}}+C_{1\varepsilon}\frac{\varepsilon}{k}C_{3\varepsilon}G_b+S_\varepsilon \tag{2.39}$$

where

$$C_1=max\left[0.43,\frac{\eta}{\eta+5}\right],\ \eta=S\frac{k}{\varepsilon},\ S=\sqrt{2S_{ij}S_{ij}}$$

Model constants:

$$C_{1\varepsilon}=1.44,\ C_2=1.9,\ \sigma_k=1.0,\ \sigma_\varepsilon=1.2$$

Likewise previous model, in these equations, G_k, represents the generation of turbulence kinetic energy due to the mean velocity gradients. G_b is the generation o turbulence kinetic energy due to buoyancy (Fluent 2005). $C_{1\varepsilon}$, C_2 and $C_{3\varepsilon}$ are constants, also σ_k and σ_ε are turbulent Prandtl numbers for k and ε. S_k and S_ε are user-defined sources terms. Furthermore considerations are presented in Cabezón et al. (2011).

For fully developed turbulent internal flow, the turbulence intensity can be estimated from following equation:

$$I=0.16\,(Re)^{-1/8} \tag{2.40}$$

Turbulent kinetic energy, k, and turbulent dissipation rate, ε, were calculated as (Versteeg & Malalasekera 2007):

$$k=\frac{3}{2}(u_{avg}\times I)^2 \tag{2.41}$$

$$\varepsilon=C_\mu^{3/4}\frac{k^{3/2}}{\ell} \tag{2.42}$$

where u_{avg} is the mean velocity inlet, ℓ is length scale a C_μ is an empirical constant equal to 0.09. Length scale depends on the length of the wind tunnel and is calculated through the following formula (Versteeg & Malalasekera 2007):

$$\ell=0.07\times L \tag{2.43}$$

where, L is the length of the wind tunnel.

Thereby, this approximation/estimation to the turbulence inputs of k - ε model model were used in this work.

2.2.5.2 k - ω Model

Another traditional turbulence model used by FLUENT is the $k-\omega$ model. The standard $k-\omega$ model is an empirical model base on model transport equation for the turbulence kinetic energy, k, and the specific dissipation rate, ω (Wilcox 1994, Fluent 2005, 2011a).

The standard $k-\omega$ model applied by ANSYS FLUENT is based on the work developed by Wilcox (1994). Over the years, the $k-\omega$ model have verified some modifications, productions terms have been added to the k and ω equations, which have concluded in the improvement of the model accuracy (Wilcox 1994, Fluent 2005, 2011a).

The main equations that govern the applicability of standard $k-\omega$ model are:

$$\frac{\partial}{\partial t}(\rho k)+\frac{\partial}{\partial x_i}(\rho k u_i)=\frac{\partial}{\partial x_j}(\Gamma_k\frac{\partial k}{\partial x_j})+G_k-Y_k+S_k \tag{2.44}$$

$$\frac{\partial}{\partial t}(\rho \omega)+\frac{\partial}{\partial x_i}(\rho \omega u_i)=\frac{\partial}{\partial x_j}(\Gamma_\omega\frac{\partial \omega}{\partial x_j})+G_\omega-Y_\omega+S_\omega \tag{2.45}$$

In these equation, likewise previous Equations 2.34; 2.35; 2.38; 2.39; G_k, represents the generation of turbulence kinetic energy due the action of mean velocity gradients, nevertheless $G_\omega$represents the production of the ω. The terms of Γ_k and Γ_ω refers to effective diffusivity of k and ω, respectively. Y_k and Y_ω symbolizes the dissipation of k and ω due to turbulence phenomena. Finally, S_k and S_ω represents user-defined source terms. All of the above terms are calculated and described more thoroughly in following literature, Fluent (2005, 2011a).

Chapter 3

Methodology

3.1 Experimental

Blade element theory was developed to measure the forces acting on different blade sections. This technique described in section 2.1.6 used to design wind turbine rotors, was not used in this work, where a detailed wind tunnel analysis were made.

3.1.1 Blade Aerodynamics

Aerodynamic models were been developed with the main objective of the evaluation of factors that may affect the prototype performance. These models are created concerning with the prototype and, a scale factor were used. Moreover, the scaling factor is considered in order to avoid some physical limitations that may exist, such as, real dimensions that some prototype may contain (White 1998). In this case, aerodynamic model of Rutland 913 blades were considered.

The modeling as analysis process must consider a likeness between the model and the prototype, this similarity is ensured by the consideration of one scale factor, L_r, defined as:

$$L_r = \frac{L_p}{L_m}$$

where, L_p and L_m, representing respectively length of prototype and model.

Thus two models with different scaling factors were implemented in wind tunnel. Model one presents a scale factor of $L_r = 6.64$ and model two presents a scale factor of $L_r = 2.81$.

The principle of physical similarity ensures that if the Reynolds number of the model is equal to the Reynolds number of the prototype, then the forces acting on the model will reproduce the forces acting on the prototype. For this case of study, was considered (White 1998):

$$Re_m = Re_P\,(=)\,\frac{\rho_m \times L_m \times U_m}{\mu_m} = \frac{\rho_p \times L_p \times U_p}{\mu_p} \tag{3.1}$$

As fluid flow model is equal to fluid flow prototype, which is atmospheric air, can be considered that $\rho_m = \rho_p = \rho$ e $\mu_m = \mu_p = \mu$, simplifying the above equation.

$$Re_m = Re_P\,(=)\,\frac{\rho \times L_m \times U_m}{\mu} = \frac{\rho \times L_p \times U_p}{\mu} = L_m \times U_m = L_p \times U_p \tag{3.2}$$

Experimental test were made in subsonic wind tunnel as can be seen from Figure 3.1. The wind tunnel used in this work is an Armfield Limited model C2 Subsonic Wind Tunnel. The structure of the wind tunnel accommodates an aerodynamic balance which evaluates the drag and lift performance, also have a fan, and a test section (Armfield 2009).

Figure 3.1: Subsonic Wind Tunnel.

Test section have an octagonal form and presents 304 mm wide x 304 mm high x 457 mm long of working volume. The aim of this experimental study it's perform an analysis of the aerodynamic performance of the drag force and lift force associated with the variation of attack angle of the wind turbine blade. Aerodynamic balance presents a sensitivity of ± 0.01 N, and is limited for 2.5 N drag values and 7.0 N for lift values (Armfield 2009).

The fan system is responsible for the insufflation of the air inside the wind tunnel test section according to a modulation imposed by the electric motor frequency inverter. Air flow velocity is directly dependent of the fan rotation frequency, this relation is imposed by the following equation.

$$U_\infty = 0.4694F + 0.28 \tag{3.3}$$

where, U_∞, is air velocity experienced in wind tunnel, and F, is the rotation frequency of the fan.

The legitimacy condition of the experimental tests are guaranteed by the principle of physical similarity with consider an equal speed test for both model's, $U_m = 20\ m/s$ corresponding to a wind speed on the prototype for model 1 of $U_p = 3.01\ m/s$ and for model 2 , $U_p = 7.12\ m/s$.

Moreover it can be stated that activities of adapting and scaling the blade models were performed. Therefore, in order to create the aerodynamic models, rotor blades were manufactured using an 3D Printer (Zprinter 310 Plus). A model made of zp130 Composite Material, as can been seen in Figure 3.2, were produced.

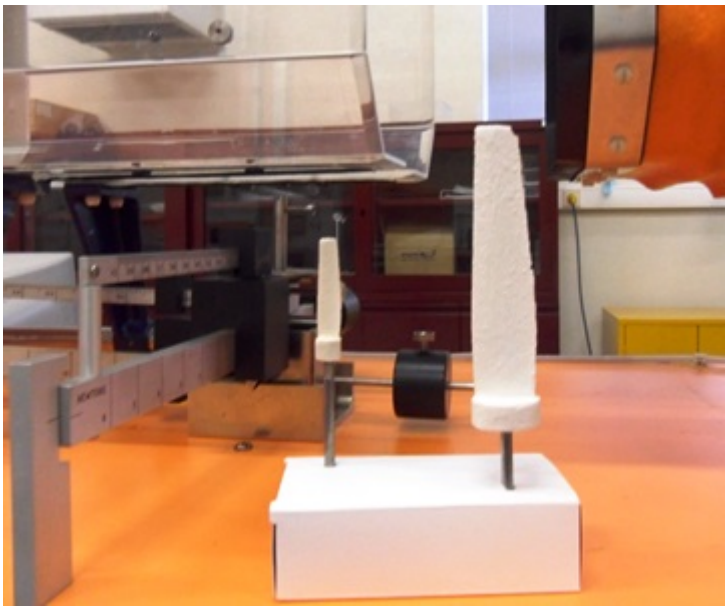

Figure 3.2: Aerodynamic models produced considering a different scaling factor.

These rotor blades present a NACA 8311 cross section based on previous choices made by Paulo (2013).

The experimental device is used to predict the aerodynamic behavior and investigate the conditions experienced by a wind turbine blade placed in the air flow. Therefore, blade axis is placed in the middle of the octagonal test section connected to aerodynamic balance. The entire tests have been conducted with a maximum value of air velocity equal to 20 m/s. Experimental measures were made considering different environmental temperatures. In this measures was obtained environmental temperature around 290.15 K.

Aiming at evaluation of drag and lift force at different attack angle positions, it was used the variation imposed by the angled ring that own aerodynamic balance. Therefore, the aerodynamic blade models were evaluated to the following attack angles: -10 º; -5 º; 0 º; 5 º; 10 º; 15 º; 20 º; 25 º; 35 º; 40 º; 45 º; 50 º; 55 º; 90 º.

3.1.2 Wind Turbine Performance

Evaluations of the generated electricity were performed in subsonic wind tunnel for different wind speeds. Application of wind turbines in urban setting are primarily characterized by the operating at low wind speeds, as such, more importance was given to these speeds. The wind turbine model was tested in the wind tunnel for the following wind velocities: 6; 7; 8; 10; 12; 14; 16 m/s, ranged from $47143 < Re < 125714$.

Corrections for a temperature value of 290.15 K and for an altitude of 600 m were made. Altitude-air density calculation was made considering the International Standard Atmosphere model. Thus, following equations were used for correction of air density value (Rashford et al. 2010).

Pressure at altitude, h, is given by:

$$P = P_0 \left(1 - \frac{Lh}{T_0}\right)^{\frac{gM}{RL}} \tag{3.4}$$

where, P_0, is sea level standard atmospheric pressure (101.325 kPa); T_0, sea level standard temperature (288.15 K); g, earth-surface gravitational acceleration (9.8067 $^{m}/_{s^2}$); L, temperature lapse rate (0.0065 $^{K}/_{m}$); R, universal gas constant (8.3145 $^{J}/_{mol \cdot K}$); M, molar mass of dry air (0.0290 $^{kg}/_{mol}$)

Air density as function of altitude can be calculated according to:

$$\rho_h = \frac{PM}{RT_{measured}} \tag{3.5}$$

In short, the new density of air was, $\rho_h = 1.1337\ ^{kg}/_{m^3}$, which to be used in the following sections.

Physical dimensions of subsonic wind tunnel allow only to evaluate aerodynamically wind turbine models with reduced dimensions. These dimensions were optimized by Paulo (2013). Also aerodynamic wind turbine model made of medium density fiberboard and aluminum developed by Paulo (2013) was used. Allied to the limited size of the model, the same have to accommodate a small 3 W electric generator. Figure 3.3 illustrates the wind turbine model used in wind tunnel measurements.

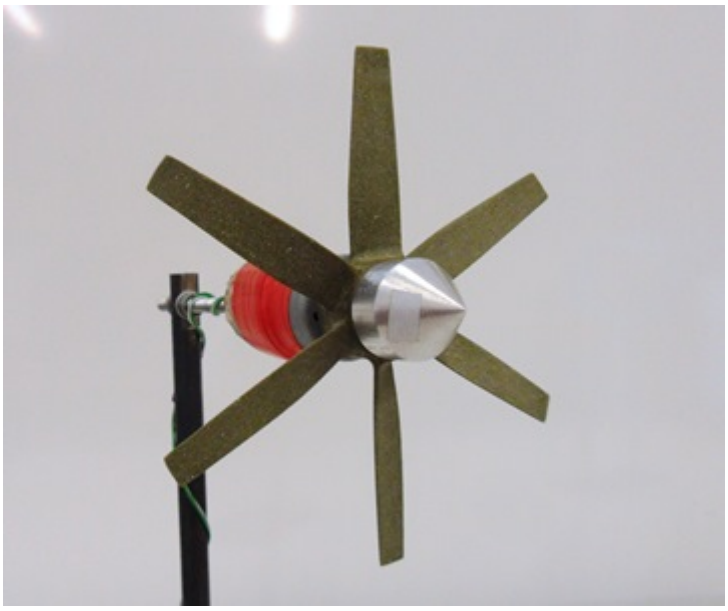

Figure 3.3: Wind turbine model used in experimental setup.

Figure 3.4 shows electrical circuit diagram used in measurements of the power generated by wind turbine.

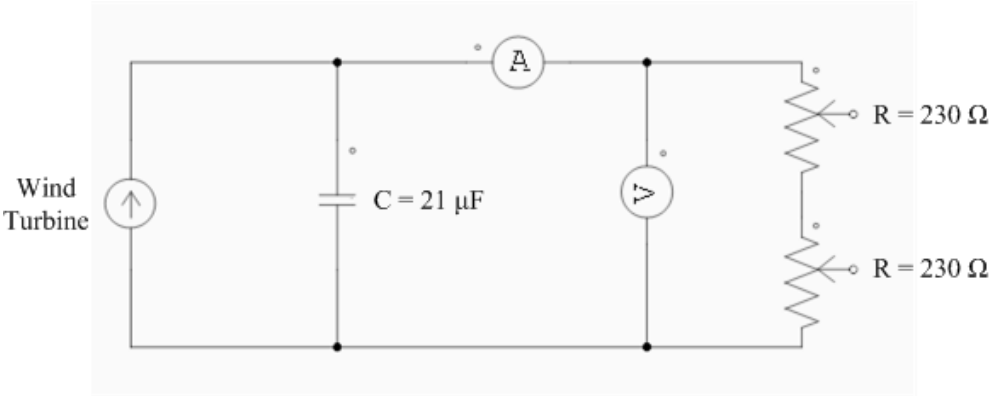

Figure 3.4: Electrical circuit diagram used to evaluate electric power generated.

Following the methodology previously proposed by Paulo (2013) it was possible to evaluate the electric power produced by wind turbine operation. It was applied a simple control algorithm, by ensuring a load variation. Additionally was considered the twice of the load considered by Paulo (2013) using two rheostats ($R = 230\ \Omega$). Throughout load variation it was feasible to identify the highest point of electric power produced by the wind turbine at each wind speed studied. At this point a speed rotation measurement was made through out an Hibok 22 digital tachometer.

In order, to enhance the electric performance of wind turbines, experiments in wind tunnel with a system composed by an encapsulated wind turbine were done. Encapsulated wind turbine system is performed accommodating a C-D that surrounding the wind

turbine, as can be seen in Figure 3.5 - 3.6. In literature an identical study with the same equipment can be found (Paulo 2013).

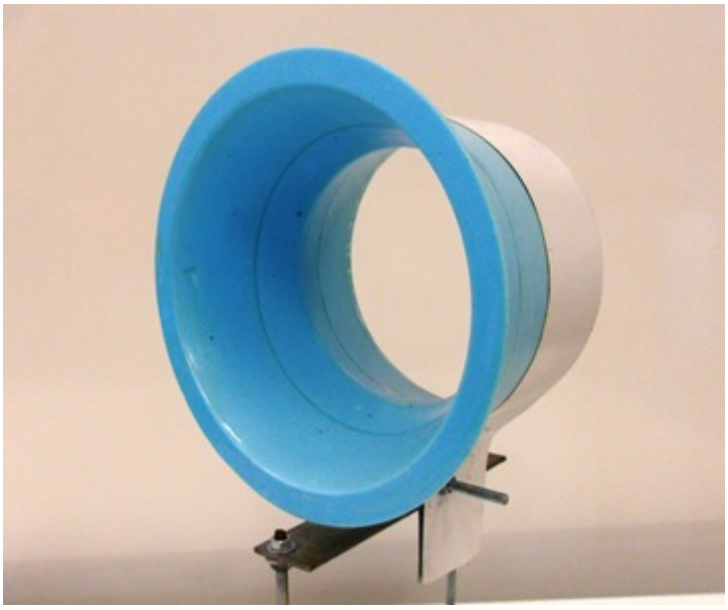

Figure 3.5: C-D system used in experimental trials.

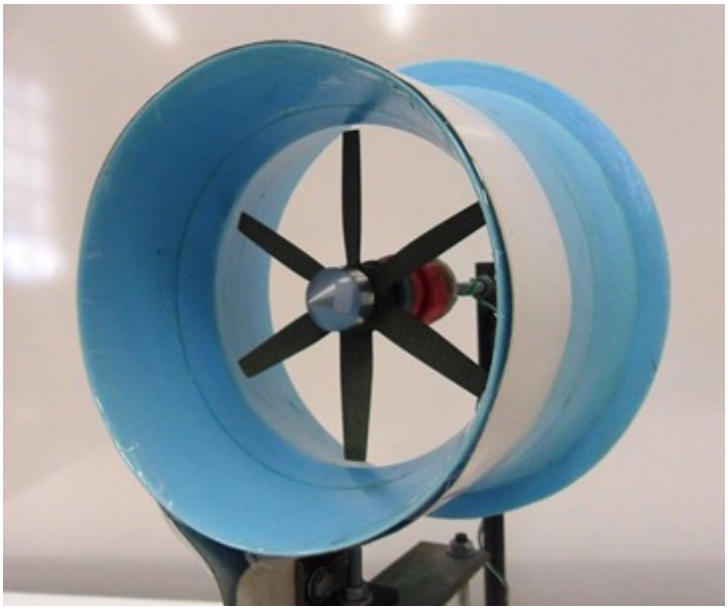

Figure 3.6: Representation of the model developed by Paulo (2013), implemented in experimental wind tunnel setup.

It's worth noticing, that C-D was constructed with extruded polystyrene (XPS). Models developed by Paulo (2013) present a scale factor of $L_r = 8.33$. Table 3.1 presents the main design dimensions.

Table 3.1: Main dimensions on the C-D model design (Paulo 2013).

Part or Detail	Dimensions
C-D length	108 mm
Diameter at C-D center	108 mm
Brim/Flange size	10 mm
Concentrator angle (α_i)	8 º
Diffuser angle (α_o)	16º

Evaluation in subsonic wind tunnel to the system composed by the encapsulated wind turbine was performed with the same methodology applied to the experimental trials made to the wind turbine.

3.2 Numerical Methodology

The main objective of the current study is to take an incremental step in the development of the aerodynamic performance of a wind turbine blade.

Present work was performed using an ANSYS FLUENT 14.5, an example of commercial CFD code.

For perform a CFD 3D model, the following steps were considered applied by Lanzafame et al. (2013) :

- Reproduction of the wind turbine blade using 3D CAD file;
- Generation of computational domain;
- Meshing of computational domain;
- Setting turbulence model;
- Defining the specifications of FLUENT solver;
- Post Processing results.

3.2.1 Blade Aerodynamics

3.2.1.1 Pre-Solver

CAD files were imported as parasolid form and an enclosure form was made to ensure wind tunnel structure. One boolean operator was done to subtract wind turbine blade in wind tunnel volume, in order to simulate only the air around the blade. The fluid has been assumed to be incompressible, being maximum fluid velocity in order of 20 m/s.

Model includes only the blade, and neither the tower and the ground were included in this model. Further considerations were done with the regard of a rotor diameter of 0.11 m.

The pre-processor ANSYS ICEM CFD 14.5 was used to build a tetrahedral mesh of approximately 1.24 million volume elements (tetrahedral form) for blade model 1 and 1.40 million volume for blade model 2. Figure 3.7 shows the blade mesh, without the presence of virtual wind tunnel structure.

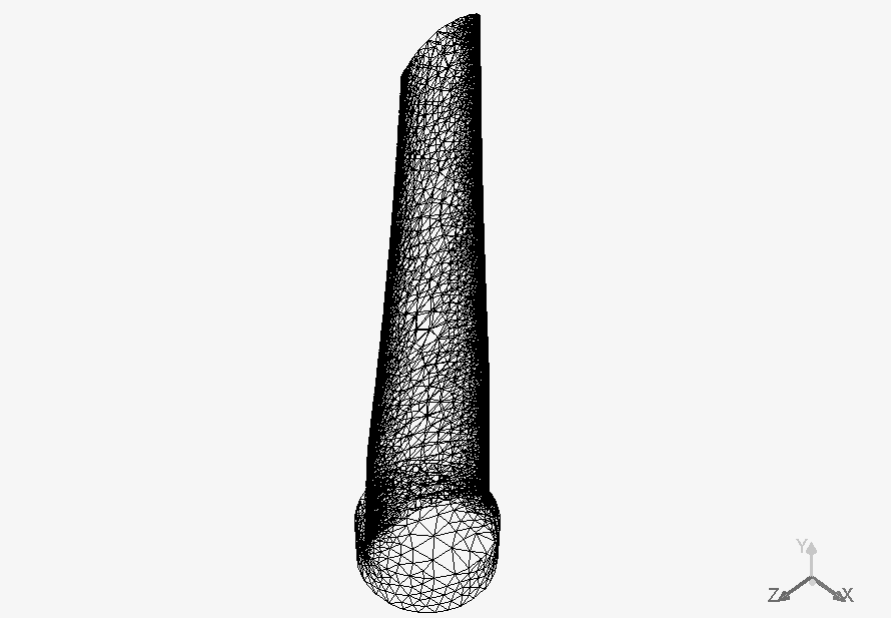

Figure 3.7: Mesh of blade computational domain, without the presence of virtual wind tunnel structure.

To ensure these approximately number of elements on each model blade, considering their different attack angles, the parameters shown in Table 3.2 were applied.

Table 3.2: Sizing Mesh details applied on generation grid for models blade.

Sizing Mesh details	
Solver Preference	Fluent
Use Advance Size Functions	On: Proximity and Curvature
Relevance Center	Fine
Initial Size Seed	Active Assembly
Smoothing	High
Transition	Slow
Span Angle Center	Fine

Others options were left default. On the wind tunnel volume was needed for applying an Independent Patch. This patch presents the Tetrahedrons Method with a 16º angle.

The whole setup was done with main objective of, due to geometric complexity, perform a mesh accurately as possible.

The dimensions of computational domain were selected to replicate some of the considerations identified in experimental component. Therefore, these dimension for wind turbine blade model 1 are illustrated in Figure 3.8 for a 5.5D x 1.8D x1.9D.

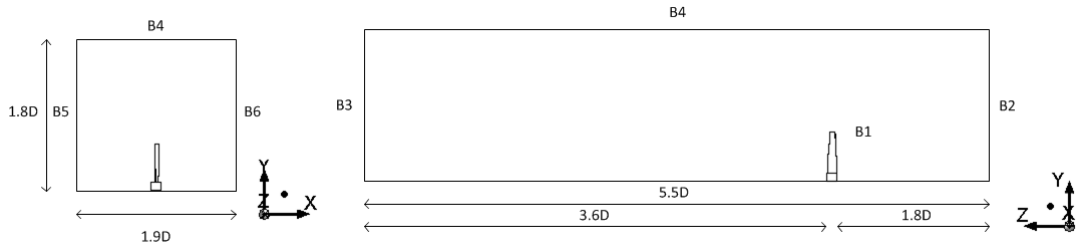

Figure 3.8: Computational domain and boundary conditions.

Table 3.3: Boundary Conditions.

Boundaries in Figure 3.8	Boundary conditions in Fluent
B1	Wall
B2	Velocity inlet
B3	Pressure outlet
B4	Symmetry
B5	Symmetry
B6	Symmetry

Figure 3.8 and Table 3.3 shows the boundary conditions imposed for a $k-\varepsilon$ arrangement.

A uniform velocity condition of 20 m/s with turbulent kinetic energy (Equation 2.41) of 1.37 m^2/s^2 and turbulent dissipation rate (Equation 2.42) of 6.27 m^3/s^3 was applied for blade model 1, as the boundary condition at the inlet where the flow enters the computational domain. For blade model 2 an uniform velocity condition of 20 m/s with turbulent kinetic energy of 1.10 m^2/s^2 and turbulent dissipation rate of 3.38 m^3/s^3 were applied. For pressure-outlet was used a constant value of Gauge pressure of 0 Pa. For the case of physical domain (Wall) a shear condition of No Slip was used.

In the case of blade model 2 in the computational domain of blade model 2 the distance between blade and pressure outlet was increased for 5.4D, due to the consideration of a blade with a smaller scaling factor. These dimensions were considered in order to accommodate the available computing resources.

Once the grid is generated, the three-dimensional Navier-Stokes equations are solved using a RANS approximation.

The choice of turbulence model is mainly affected by the type of problem and also by the relation between desired accuracy and computational resources available (Sumner et al. 2010).

However, most of the simulations need to at least make a forecast of the general shape of the velocity profiles as well as locate main vortices generated (Krogstad & Eriksen 2013).

For the wind turbine blade aerodynamic performance development a traditional turbulence model was implemented. In this way, in each cases a $k-\varepsilon$ realizable model was used, combining with an enhanced wall treatment on the near-wall treatment. The default constant models were considered.

3.2.1.2 Solver

The pressure-based solver is set as it's traditionally used for problems including incompressible flows (Fluent 2011*a*, Makridis & Chick 2013).

All simulations were performed with an Intel (R) Core (TM) i7-4770 CPU@3.40GHz Processor with a total installed capacity of 12.0 GB of RAM.

Pressure-velocity coupling is achieved with the SIMPLEC algorithm, in order to allow faster convergences. Gradient in spatial discretization of Green-Gauss Node-Based was used to ensure results more accurate (Fluent 2011*a*). The second order scheme is used for pressure calculations.

Third-order MUSCL discretization is chosen for momentum equations and turbulence equations including turbulent dissipation rate and turbulent kinetic energy equations are discredited using second-order upwind scheme. For time integration, the second order implicit formulation is used.

In FLUENT simulations, it's relevant to monitor the process to verify when solution is converged (Lanzafame et al. 2013). For this work, three monitors were used: Residuals monitors of the process; a trend of lift coefficients, C_L, as function of time step; and a monitor to verify the drag coefficient trend, C_D, as function of time step.

The convergence criteria used for continuity and momentum was an absolute criteria of 10^{-4}. For turbulence quantities an absolute criteria of 10^{-3} was used.

All simulations were performed with a time step intervals of 1 second with a total 200 time step and considering a maximum 20 iterations / time step. However if convergence is not achieved for these conditions, a controlled reduction was applied on under-relations-factors. Posterior is given continuity to simulations until it's verified convergence solution.

3.2.2 Wind Turbine Performance

Wind turbine performance for the various rotational speeds and air flow conditions were studied using a 3D model that replicates the physical dimension of the aerodynamic model tested at wind tunnel. Instead of subsection 3.2.1, the procedure on the rotor performance includes motion of elements. Therefore, rotational motion needs to be considered.

FLUENT solver have available different ways to modeling rotational effects. The choice of rotational model has to evaluate physics complexity of the problem and computational resources available. Regarding this considerations, FLUENT presents three rotational models: Moving Reference Frame; Sliding Mesh Model and Dynamic Mesh Model (Lanzafame et al. 2013, Fluent 2011*a*).

Taking into account, motion of elements high computational resources for mesh generation/refinement become essential (Lanzafame et al. 2013).

Nevertheless, CFD calculations were performed to evaluate the effects that C-D device produces in air flow.

3.2.2.1 Pre-Solver

Wind turbine 3D CAD file was imported as parasolid form and an enclosure form was generated to ensure the surrounding air. Figure 3.9 shown the computational domain performed in Design Modeler.

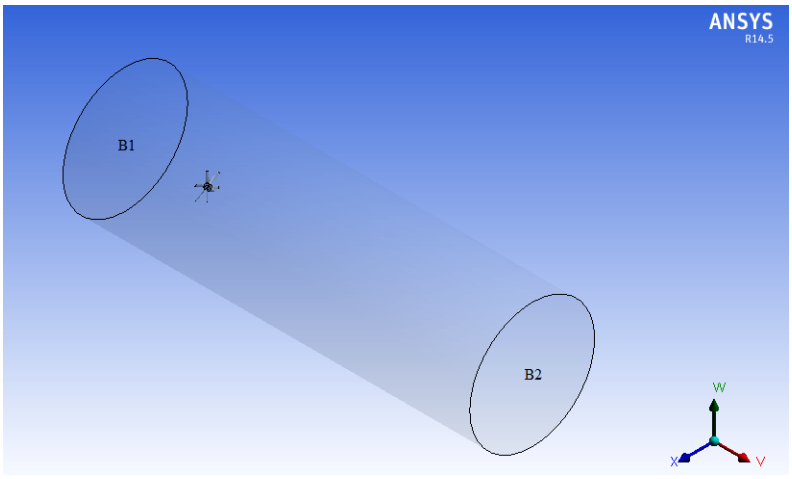

Figure 3.9: Computational domain produced with the enclosed wind turbine (B1 - velocity-inlet and B2 - pressure-outlet).

As can been seen from Figure 3.9 a cylindrical domain with a radius of 0.2 m was created. Moreover, the distance of the rotor relative to the inlet and outlet of the domain, were taken into account. Therefore, following Figure 3.10 produce these distance specifications, which were:

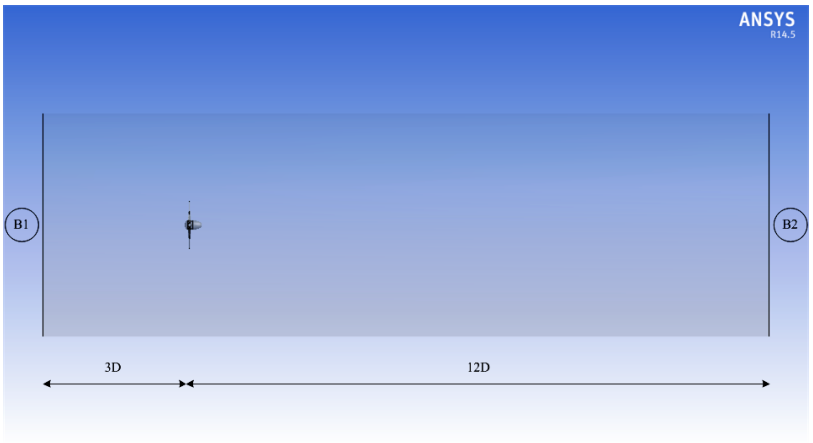

Figure 3.10: Computational domain specifications, WT distance relative to velocity-inlet (B1) and with pressure-outlet (B2).

Current distance of 3D and 12D relative to the inlet and outlet boundary, was selected based on the work developed by Carcangiu (2008), Gomis (2011), Fleck (2012), Mo et al. (2013). Therefore, these intervals are considered suitable for the simulation of the wind turbine performance.

As in previous subsection, pre-processor ANSYS ICEM CFD 14.5 was used to build a tetrahedral mesh of approximately 1.3 million elements (tetrahedral form). Figure 3.11 shown the performed mesh.

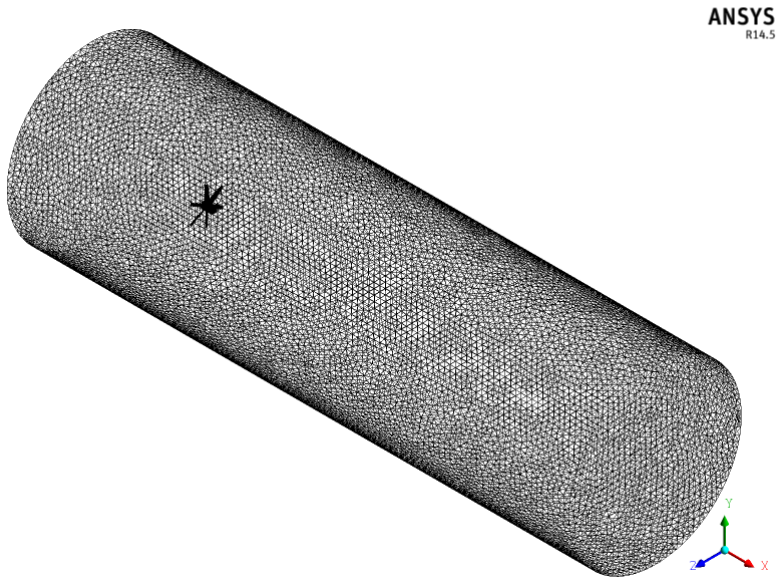

Figure 3.11: Computational mesh generated for the analysis of rotor performance.

As presented in Figure 3.11 a cylindrical mesh was created containing in it's interior the wind turbine domain. Moreover, the mesh referring to rotor was generated with a smaller element size relative to the surrounding air.

Several considerations in pre-processor were applied with main objective of produce

an accurately mesh as possible. Due to the geometry complexity, and rotational effects that needs to be considered, grid generation phase should be regarded with some attention. The parameters presented in Table 3.2 were applied, to produce the presented mesh.

The computational mesh produced was created with the intention of generating reduced computation times, thus two independent patch were applied, respectively, to the parties that form the domain. Controls were applied with a tetrahedrons method and different size elements were used to refine the performed mesh.

Upon completion of the mesh creation phase, the three-dimensional Navier-Stokes equations are solved using a RANS approximation. A standard $k-\omega$ model was used with the default options presented by the model on the software package.

As stated previously, CFD calculations were conducted to analysis of effects that C-D device generates in the air flow that surrounding the wind turbine. The C-D 3D CAD file was imported as IGES file and were reproduced the domain dimensions applied as in the case of wind turbine. Figure 3.12 shown the computational domain performed in Design Modeler.

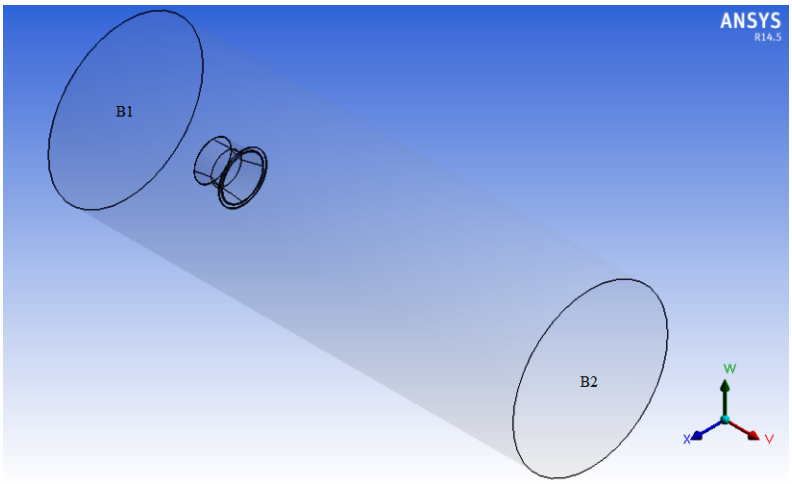

Figure 3.12: Computational domain produced with the enclosed C-D (B1 - velocity-inlet and B2 - pressure-outlet).

As considered suitable for the simulation of wind turbine performance, then those dimensions were chosen to produce a computational domain as described in Figure 3.12.

Subsequently, a tetrahedral mesh of approximately 2.8 million elements (tetrahedral form) was produced using pre-processor ANSYS ICEM CFD 14.5. Following Figure 3.13 presents the performed mesh.

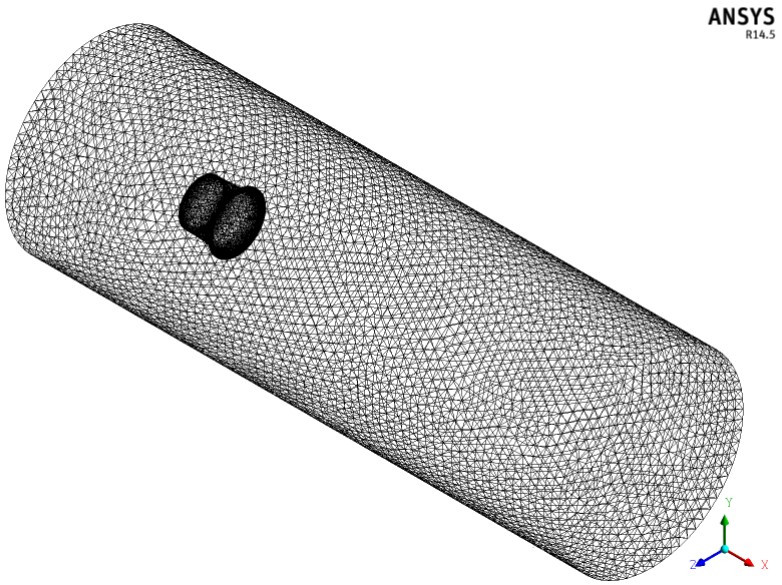

Figure 3.13: Computational mesh performed for the analysis of effects that C-D generated in air flow.

As presented in Figure 3.13 the C-D domain was generated with a smaller element size than surrounding air flow.

Turbulence modulation effects as previously a standard $k-\omega$ model were used.

3.2.2.2 Solver

To increase the computing power a parallel processing was applied where 4 CPU were used.

A pressure-based solver with a transient formulation was applied with a density of the air $\rho_h = 1.1337\ {}^{kg}/_{m^3}$.

Regarding to the modulation of the rotational effects, on this work the moving reference frame was implemented. To setup the frame motion model, the unit vectors and origin of the rotation axis were imposed. The cell zone condition was set up by imposing the rotational velocity in the absolute specification. The values imposed are described in Table 3.4. Through equation 2.17, the optimal angular speed that wind turbine generates can be described. Throughout, a design parameter described in Paulo (2013), a tip speed ratio equal to $\lambda = 2$, as defined in equation 2.17 was considered. Therefore, the optimal values of angular speed rotor are shown in Table 3.4

Table 3.4: Optimal angular speed that rotor generates.

Wind speed [m/s]	Angular Speed [rad/s]
6	222
7	259
8	296
10	370
12	444
14	519
16	593

Values presented in Table 3.4 describes a somewhat importance due to their use as inputs in the methodology applied in FLUENT.

Wall motion of the wind turbine blades, describes a rotational motion relative to adjacent cell zones. Hence, unit vectors and origin of the rotation axis were described again. The wall boundary condition for the rotor had a zero relative speed with respect to adjacent cells. Relatively, to the boundaries conditions of the wind turbine model, no slip condition accounting for wall velocities were imposed.

Relatively to, the solutions methods in the pressure-velocity coupling SIMPLE scheme was used. Spatial discretization methods used are presented in following Table 3.5.

Table 3.5: Methods applied in spatial discretization solutions.

Spatial discretization	
Gradient	Least Squares Cell Based
Pressure	Standard
Momentum	Second order upwind
Turbulent kinetic energy	Second order upwind
Specific dissipation rate	Second order upwind

Lastly, in transient formulation, the first order implicit methods were implemented in the calculations performed for the wind turbine performance. Regarding of solutions controls, the default values were used.

The convergence criteria used for continuity was an absolute criteria of 10^{-4}. Based on CFD theory, and according with Moshfeghi et al. (2012) this range is not sufficient, but for HAWT cases, a better convergence is notoriously very hard to achieve.

Calculations were preceded by an hybrid initialization. Subsequently, simulations were performed with a time step intervals of 0.001 second with a number of 50 time step and considering a maximum of 30 iterations/time step. Furthermore, simulation was given to continuation with a time step intervals of 0.0005 second with a number of 50 time step and considering a maximum of 30 iterations/time step.

Relatively to numerical calculations concerning to C-D device the same methodology was used and simulations were performed with a time step time step intervals of 0.01 second with a number of 150 time step and considering a maximum of 20 iterations / time step. Subsequently, to fulfill the convergence conditions was realized a simulation with a time step time step intervals of 0.001 second with 25 time step.

Chapter 4

Results and Discussions

4.1 Experimental

4.1.1 Blade Aerodynamics

Blades aerodynamics presents a somewhat importance in the performance of wind turbines. Therefore, studies need to be made in order to take an increment step in the aerodynamic performance of wind turbines. Thus, an evaluation of the drag and lift force performance were implemented.

Experimental tests in wind tunnel were made to understand the specific effects of drag and lift force on the wind turbine blade. To study the forces that act on wind turbine blade prototype at a two level of wind speed, two aerodynamic models were used, leading to a $U_p = 3.01\ m/s$ for aerodynamic model 1 and $U_p = 7.12\ m/s$ for aerodynamic model 2.

Throughout this work, the study of drag and lift force effect was made for different attack angles. Tables (4.1-4.2) present statistical results of the measurement results. The following table depicts the experimental results obtained in the study of aerodynamic model 1 drag and lift forces.

Table 4.1: Drag and lift force values (N) obtained in the evaluation of aerodynamic blade model 1.

Attack	$F_D \times 10^3$		$F_L \times 10^3$	
Angle (º)	Mean (N)	Standard Deviation (N)	Mean (N)	Standard Deviation (N)
-10	56	5	16	8
-5	51	4	14	5
0	49	4	13	5
5	44	5	7	5
10	49	4	3	5
15	50	0	16	5
20	51	4	23	5
25	56	5	33	5
35	67	5	44	5
40	76	5	46	8
45	83	5	44	5
50	93	5	46	5
55	100	0	41	7
90	139	4	13	5

In Table 4.1 the principle statistics (mean; standard deviation) derived by the experimental tests made on aerodynamic model 1, focusing the study of the drag and lift was analyzed . In this table is verified that the mean values of drag force increase with the variation on attack angle. Relatively to the standard deviation values ranging between 0.004 N and 0.005 N, except the values that corresponding to the 15º and 55º. These present a standard deviation of null due the same value on various measurements was obtained.

As like in the case of drag force values, a small values of lift force were measured, due to the small size and thickness that the blade own. Furthermore, it's worth noticing a slight variation in standard deviation values. These range between 0.005 - 0.008 N.

Focusing on aerodynamic study of blades performance, an analysis with aerodynamic model containing a smaller scaling factor was done. It becomes possible to evaluate higher forces values due to the consideration of a model with higher dimensions. Therefore, the following Table 4.2 shows the experimental results obtained on the wind tunnels tests performed on the aerodynamic blade model.

Table 4.2: Drag force and lift force values (N) obtained in the evaluation of aerodynamic blade model 2.

Attack	$F_D \times 10^3$		$F_L \times 10^3$	
Angle (°)	Mean (N)	Standard Deviation (N)	Mean (N)	Standard Deviation (N)
-10	181	19	121	12
-5	150	16	94	5
0	121	16	53	21
5	100	13	49	23
10	83	5	236	29
15	90	6	351	19
20	101	20	377	51
25	131	18	433	18
35	226	20	467	20
40	269	17	447	18
45	336	15	431	13
50	390	12	410	12
55	434	13	404	13
90	833	8	106	15

As expected, a larger model is subjected to a higher drag force values. The same behavior is observed for lift force values. Considering an aerodynamic model of smaller scaling factor imposes a larger fluctuation on the standard deviation values.

In short, in this work has used a rotor designed to work in places characterized by low wind speeds values. Therefore, this study has it's importance, in the resultant forces that the blades are subjected.

4.1.2 Wind Turbine Performance

Experimental measurements were performed in wind tunnel, in order to evaluate the electric performance of a wind turbine. In short, electric power values were obtained at different values of prevailing wind.

Following power coefficient theory an aerodynamic performance of wind turbine operation can be performed. Thus, a study of extracted power by the turbine needs to be evaluated. Therefore, in Figure 4.1 are described the average results obtained in wind tunnel measurements of extracted electric power by the wind turbine. Also in the same figure a confrontation with some values present in literature is made.

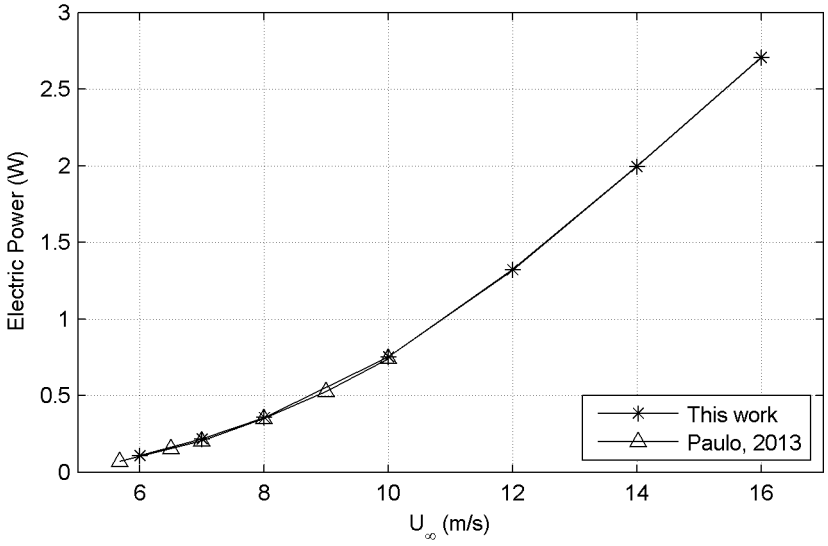

Figure 4.1: Experimental electric power generated by the aerodynamic model in wind tunnel trials.

According to Paulo (2013) due to inertia of the generator that aerodynamic model own, it's only possible to check production for values exceeding 5.68 m/s. Taking that into account the extracted electric power was evaluated for an initial wind speed of 6 m/s. Figure 4.1 presents the electric power generated from wind speed of 6 to 16 m/s. A good agreement was obtained with the values described in Paulo (2013), where experiments were made with the same equipment. In the work developed by Paulo (2013) was given more emphasis to lower wind speed values.

Moreover, new values were obtained in this work measured for larger flow velocities. These new data allows to make a more comprehensive study, and it's given a larger resolution in the zone where lower wind speeds values are presented.

The phenomenon of energy generation by the turbine is governed by the variation of rotational speed that is obtained by the action of wind speed on the rotor. In Figure 4.2 shows the rotational speed values measured using a digital tachometer and against with the data obtained from Paulo (2013). Unsteady effects were verified in experimental tests and error bars are used to indicate maximum and minimum values obtained.

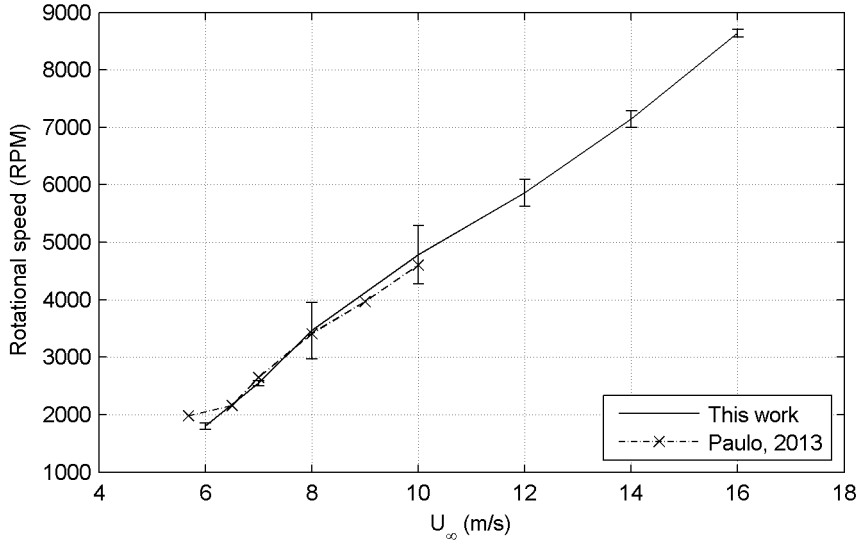

Figure 4.2: Errorbar graph of rotor rotational speeds obtained relative to those described in Paulo (2013).

As can been seen from Figure 4.2 a clear behavior of linear growing is described in the data of rotational speed as the function of wind speed values. As in the case of electric power values extracted from the rotor rotational speed values are in agreement with those obtained on Paulo (2013).

Power coefficient study shown a somewhat important on description of power performance of wind turbines. Furthermore, regarding to values obtained in wind tunnels tests, in Figure 4.3 corresponding values of power coefficient are presented.

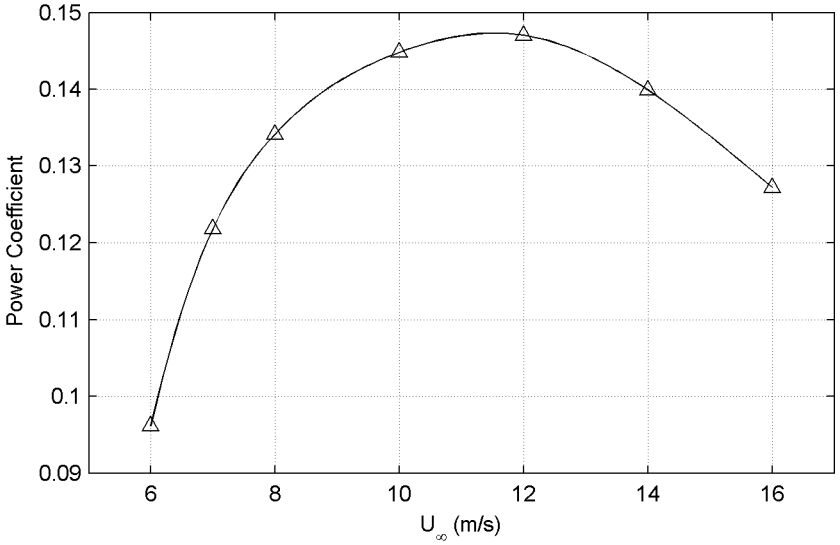

Figure 4.3: Wind Turbine power coefficient performance as function of different wind speed values.

Performance of the wind turbine was evaluated in terms of the relation between power

coefficient with wind speed values, describing a performance curve. According to performance curve shown in Figure 4.3, calculated based on the equation 2.13, a maximum power coefficient at approximately 12 m/s is obtained. Moreover, at higher wind speed values a reduction of power coefficient values is verified. Nevertheless, in the case of lower wind speed, the lowest power coefficient values are obtained. Despite of some associated errors in the experimental measurements, it's possible to consider that the data of power coefficient is approximated to the American Wind Turbine performance curve, depicted in Figure 2.4.

In order to investigate the energy performance of adapted wind turbine with a concentrator - diffuser, experimental tests in wind tunnel were done. As intend to conduct a confrontation of the energy performance of the two analyzed situations the same wind speeds conditions were replicated. Due to experimental difficulties, it was not possible to determine the electric power produced for 16 m/s. As in the previous situation, the electric power produced was evaluated with the aim to determine the coefficient of performance. The results obtained in this work were also compared with other data published in the literature obtained by Paulo (2013), where equal experimental measurements for wind speed values of 5.68; 6.5; 7; 8; 9; 10 m/s were made.

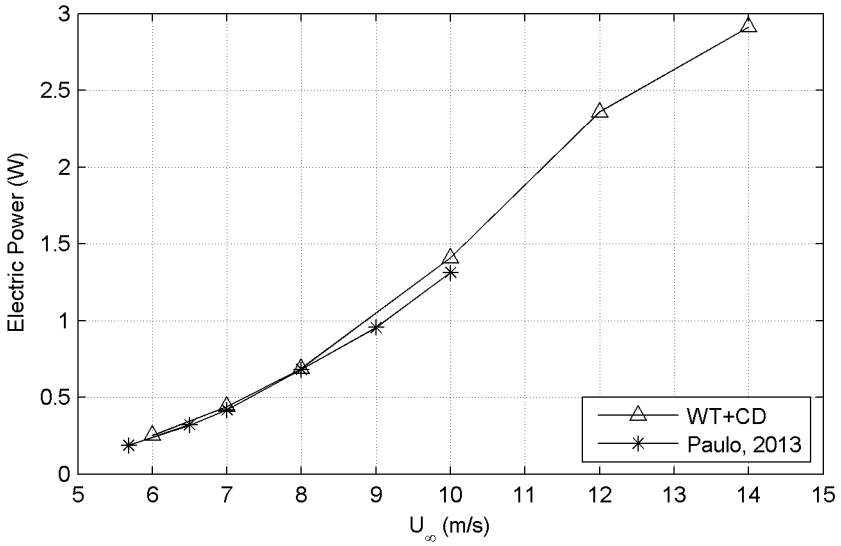

Figure 4.4: Experimental electric power generated by the implementation of shroud in wind tunnel trials ($\triangle$) compared to those described in Paulo (2013) ($*$) .

As can be seen in Figure 4.4, electric power values describe a good agreement to those obtained in Paulo (2013). Data describes a particular resemblance for smaller wind speed values. Experimental trials make it possible to describe a complete behavior of the electric power produced by wind turbine combined with C-D device. In this case, a significant growth continues to be described in electric power values. Moreover, it's becoming clear that the behavior that C-D induces in electric power production of wind

turbine is the enhancement of productivity. Thus, a comparison of electric power generation in both conditions studied becomes notorious an improvement behavior. Therefore, this comparison is described in following Figure 4.5.

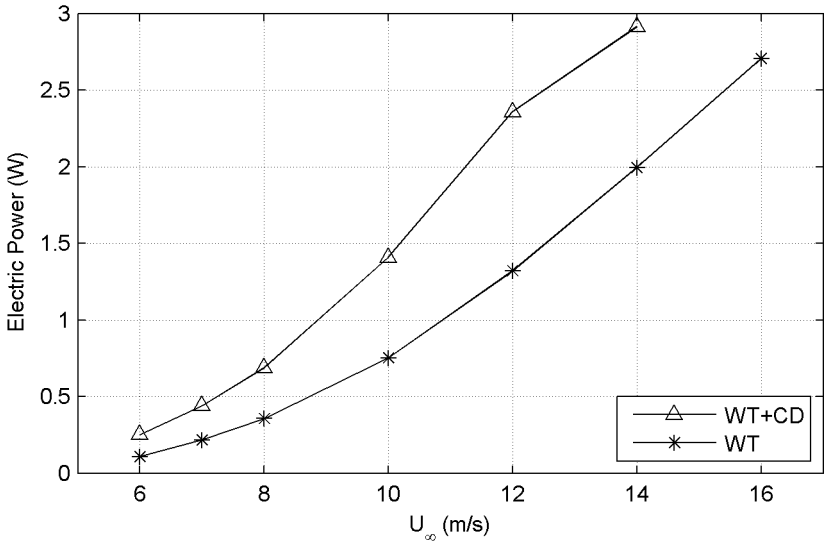

Figure 4.5: Electric power values in function of wind speed, in the case of Wind Turbine ($*$) and Wind Turbine adapted with a Convergent-Diffuser ($\triangle$).

The main objective of C-D association is to generate significant improvements in production output. As can be seen from Figure 4.5, this goal was achieved. In fact, adaptation of C-D can produce an enhancement in electric power, caused by the concentration and acceleration of air flow that surrounding wind turbine. C-D application can effectively produce increments in air flow acceleration conclude in a somewhat enhancement in power output. Following Table can support the increment that implementation of C-D produces in production of wind turbine.

Table 4.3: Comparison of electric power production data in function of wind speed values obtained for both situations.

	Wind speed (m/s)						
	6.00	7.00	8.00	10.00	12.00	14.00	16.00
WT (W)	0.11	0.22	0.36	0.75	1.32	1.99	2.71
WT+C-D (W)	0.25	0.44	0.69	1.41	2.36	2.91	—
Variation (%)	127 %	100 %	92 %	88 %	79 %	46 %	—

It's worth noticing, as shown in Table 4.3, C-D device produces in wind tunnel experiments a maximum increase of 127 % and an average increase of 89 %. In short, the implementation of C-D produces improvements in electric power for all wind speeds studied, nevertheless, is more pronounced for lower wind speeds.

As previously stated, power coefficient plays an important role on the evaluation of wind turbine performance. Thus, in following Figure 4.6 are presented the power coefficient performance as function of different wind speed values, of the resultant experiments made to the wind turbine and to the wind turbine combined with concentrator-diffuser.

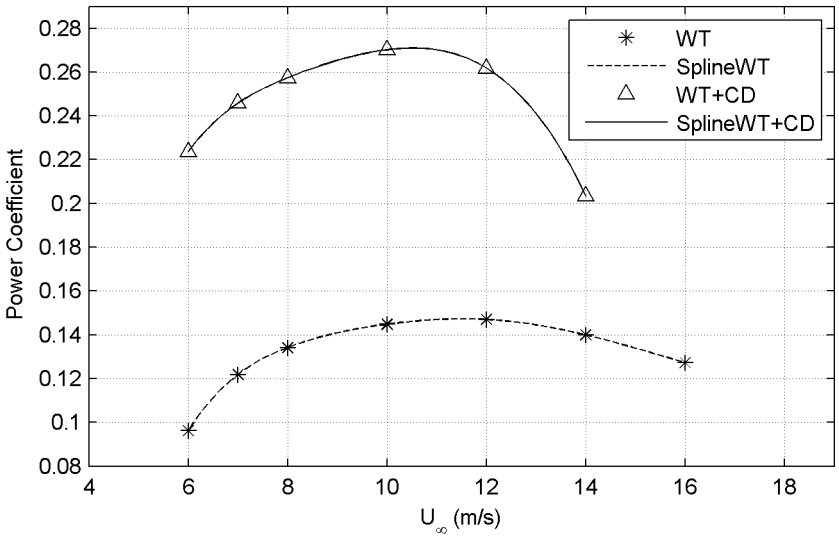

Figure 4.6: Evaluation of power coefficient performance performed to the Wind Turbine ($*$) and Wind Turbine combined with Concentrator-Diffuser ($\triangle$) in function of wind speed values.

According to the performance curve presented in Figure 4.6, a performance widely superior is described in the curve of wind turbine combined with C-D relative to wind turbine operation.

Design that C-D displays is one of the main factors responsible for the performance augmentation. Thus, concentrator and diffuser angle were optimized for produce augmentations more pronounced for lower wind speed. Therefore, with C-D implementation a maximum power coefficient is attained at lower wind speeds values, describing at this case a maximum power coefficient at 10 m/s, relatively to a maximum power coefficient achieved at 12 m/s for the case of wind turbine operation. Efficiency curve that generator presents is responsible for the take-off verified on the power coefficient performance in the values of $U_\infty = 12$ to 14 m/s.

These results help to highlight, that with the C-D implementation is possible to extract a maximum power coefficient on the wind turbine production considering lower values of approaching wind.

Furthermore, C-D implementation induces increments in power coefficient performance for all of the wind speeds values experienced. In spite of this, is verified that for lower wind speed values a higher power coefficient value is achieved relative to higher wind speed values, opposite behavior at wind turbine operation is verified. Therefore, these considerations helps to evidence that C-D implementation in small wind turbine en-

hance the wind turbine performance comparative to a conventional small wind turbines. Additionally, at lower wind speed values a higher improvement at wind turbine performance is verified. Furthermore, the Table 4.4 it's possible to verify the coherence of these affirmations.

Table 4.4: Comparison of power coefficient data in function of wind speed values obtained for both situations.

	Wind speed (m/s)						
	6.00	7.00	8.00	10.00	12.00	14.00	16.00
WT	0.10	0.12	0.13	0.14	0.15	0.14	0.13
WT+C-D	0.22	0.25	0.26	0.27	0.26	0.20	—
Variation (%)	120 %	108 %	100 %	93 %	73 %	43 %	—

Values presented in Table 4.3 describe an enhancement of the wind turbine performance, more pronounced at lower wind speed values. Moreover, Table 4.4, shown a maximum increase of 120 % and an average increase of 90 %. Thus, following the high potential for exploration that urban environment presents small wind turbines associated with C-D devices can become effectively part of the solution for production of electric energy.

These results further support the enhancement that C-D produces into wind turbine performance. Further, these devices can be used effectively at low cut-in speeds and offer improvements in energy capture when compared to a small wind turbine.

4.2 Numerical Simulations

4.2.1 Blade Aerodynamics

The issue of the aerodynamic study of the blades can be exported advantageously for CFD calculations. With the facilities produced can be given an increment in this study with the confrontation with experimental measurements. Thus, simulations were carried out for the same airflow velocities, 20 m/s presenting a Reynolds number of $Re_{M1} = 15714$ and a $Re_{M2} = 37143$, and in a wide range of attack angles (-10º to 90 º).

The computational time spent were 2 - 6 h for aerodynamic blade model 1 expect in simulation of 45º that was 14 h due to limitations that have been found to reach convergence. For aerodynamic blade model 2 computational time were range from 4 - 7 h except the cases of 40º, 45º and 50º that were ranging from 9 - 16 h.

Likewise in the experimental tests, an evaluation of drag and lift force behavior were done. Such results are presented in section 4.3 to a better comprehensive evaluation.

Along this chapter, it will become clear that the behavior of pressures acting on aerodynamic models blades studied are similar in both models. Thus, the computed pressure

coefficient distributions of the aerodynamic blade model will be present in this work.

Contours of computed pressure coefficient along the turbine blade are shown in Figure 4.7 and 4.8. Moreover, these contours refer, to blade surface model 2 and 1, respectively, for some of the attack angles investigated. The differences between the cases studied are most pronounced on the pressure side.

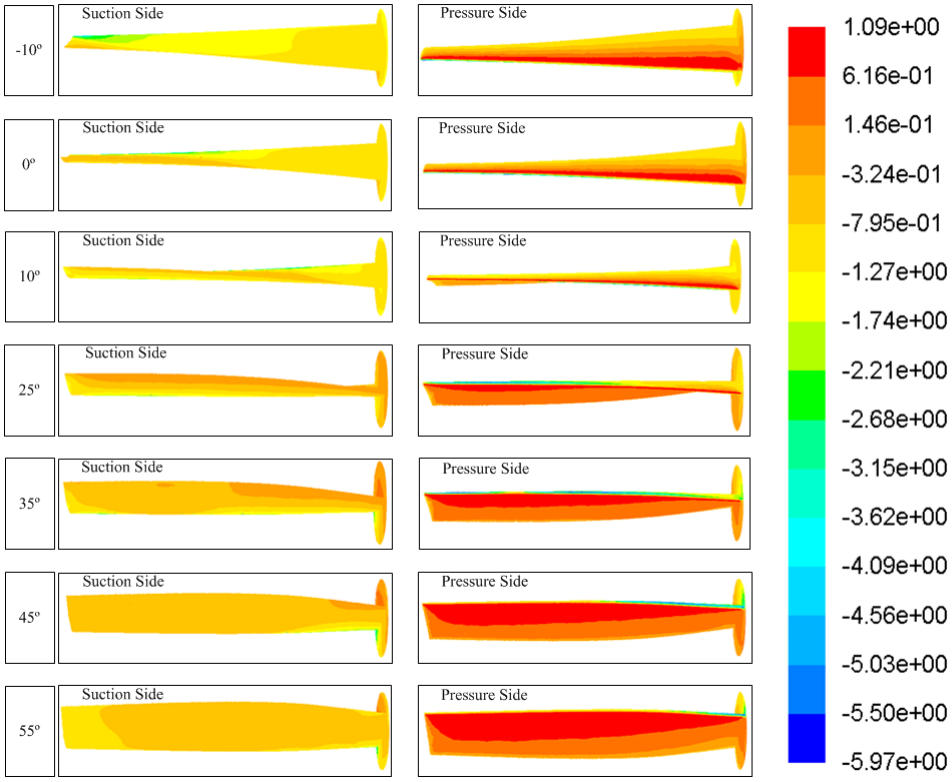

Figure 4.7: Computed Pressure Coefficient distributions on the aerodynamic model blade 2.

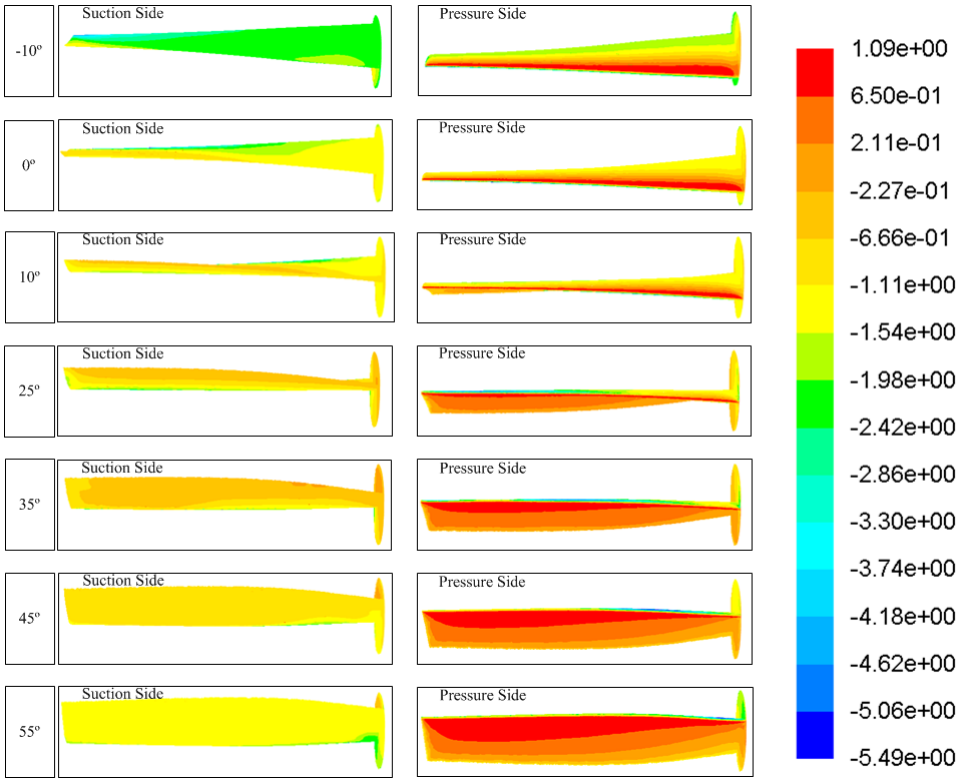

Figure 4.8: Computed Pressure Coefficient distributions on the aerodynamic model blade 1.

As suggested by previous Figures 4.7-4.8, it can be seen the relative pressures throughout a flow field around the blade (pressure side and suction side). Possibly the values presented are inflated due to the use of free stream velocity, normalizing the values of pressure coefficient.

The twist of the blade produces a large variation in the distribution of pressures on the blade. The pressure side of the blade characterized by naturally having a positive pressure values, which becomes more marked with the increasing of attack angle. On the other hand, it's visible on the figures relative to pressure side negative pressure values. The cause for the presentation of these values reside in the consideration of some attack angles, where is visible some part of the suction side.

On the suction side, the variation of the attack angle does not show great variation in the blade distribution pressures. Although, for the -10º is visible at the tip blade a marked reduction of the pressures distribution values.

Relatively to distributions of pressure coefficient of aerodynamic blade model 1 (Figure 4.8), is verified a similar behavior, although for the cases of low attack angle (-10º and 0º) occur more marked variation in pressures distribution values, even verifying the occurrence of lowest values.

The turbulent kinetic energy distribution on the blade surface is a good indicator of the turbulent energy presents in the surface.

To achieve a more detailed understanding of the flow on the suction and pressure sur-

face of the blade, the streamlines overlapping with turbulence kinetic energy distribution for both suction and pressure surface with the consideration of different attack angles are shown in Figure 4.9 and 4.10. Streamlines indicates the flow direction adjacent to the blade surface, therefore are present on these Figures.

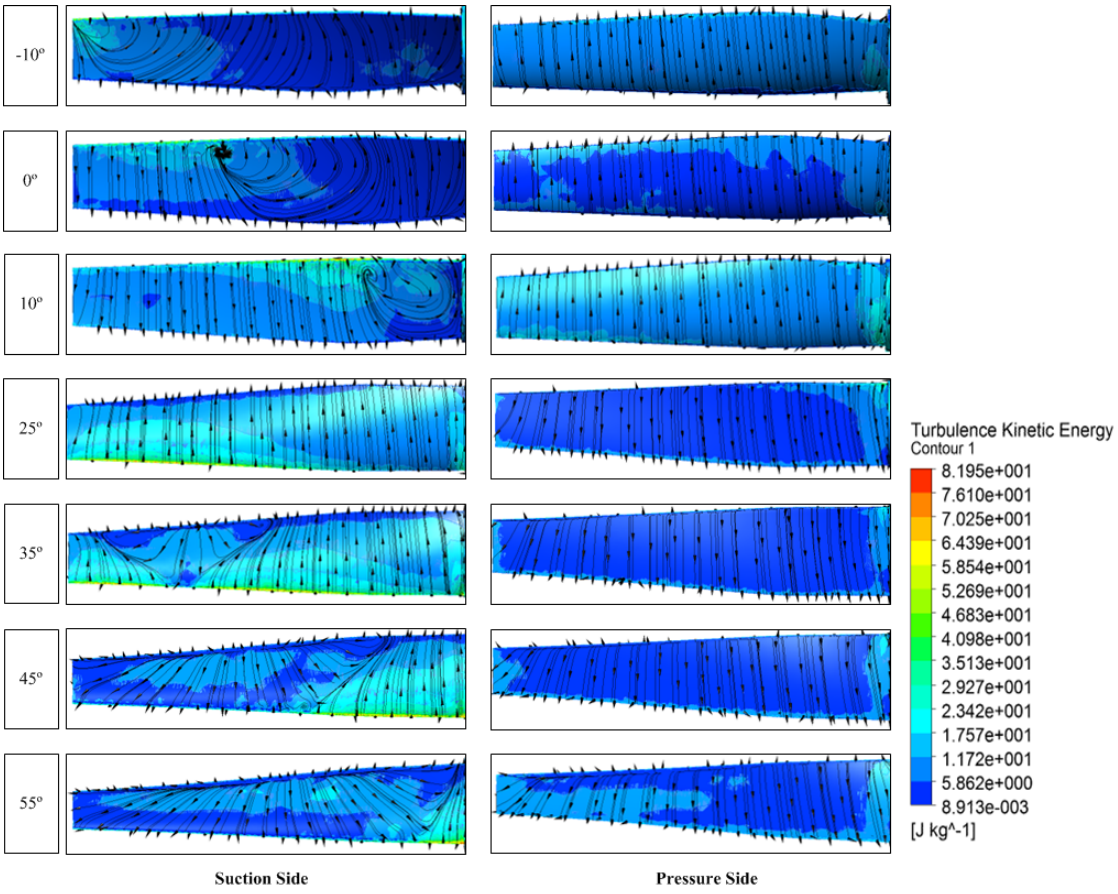

Figure 4.9: Blade surface turbulence kinetic energy plots overlaid with surface streamlines, for blade model 2.

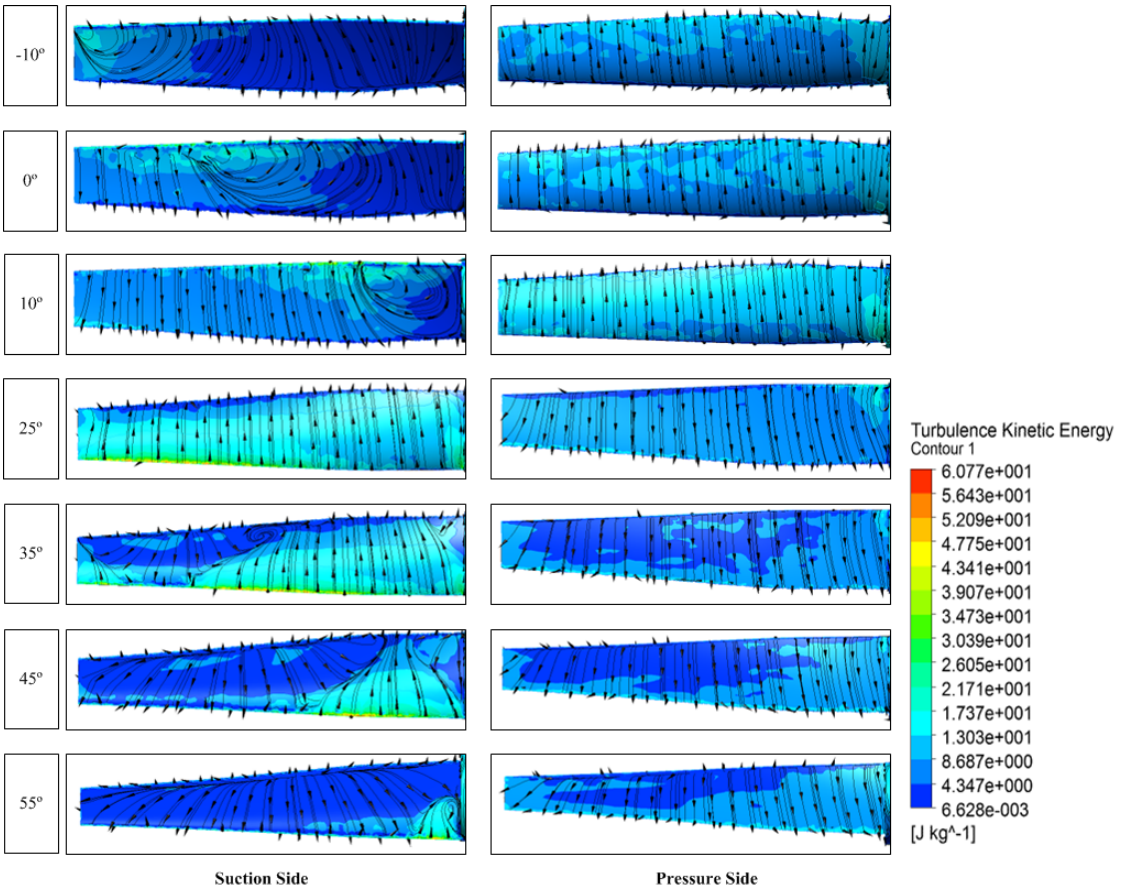

Figure 4.10: Blade surface turbulence kinetic energy plots overlaid with surface streamlines, for blade model 1.

The comparison between resultant of two aerodynamic models produces a similar behavior at surface streamlines level. Naturally, it was expected verify this similarity, due to study being about of the same aerodynamic model, but with the consideration of different scaling factors.

The same conclusion at turbulence kinetic energy level is not possible to verify. Once, as aerodynamic model 2 presents higher dimensions makes it more susceptible to consider somewhat superior levels of turbulence energy.

Due to blade twist, with the variation of attack angle, which have be made taking as reference the superior section of blade tip produces streamlines with different spanwise/streamwise directions as can be seen in Figure 4.9 and 4.10.

Pressure side of the blade is characterized as being covered with fully attached flow with no spanwise velocity component even in small area near the rotor.

In suction side of the blade, at streamlines level a different behavior is verified, due to attack angle variation.

Starting with the -10º case, there is evidence formation of radial flow at 30 to 40 % of the span length from tip to root (0º and 10º cases), leading to a fully detached flow in 25º case. Furthermore, the center of radial flow matches with zones where it's noticing a

higher value of turbulence kinetic energy.

For 35º, 45º and 55º cases, this radial flow is not observed, but a formation of boundary layer separation becomes visible. Ranging this separation with the increment of attack angle from tip to root blade.

It's worth noticing, with a careful view that became possible to observe the formation of streamline complexity in leading edge location. This unexpected streamwise presents a limitation on the suction side for a high attack angle (55º).

4.2.2 Wind Turbine Performance

In attempt to evaluate the wind turbine performance through computational tools, CFD calculations were implemented. The computational time spent for each of the simulations ranged between 2 and 3 hours.

Calculations were performed with the main objective of extract the numeric torque that wind turbine generates at different wind speed values. Therefore, with numerical torque was attempt to attain wind turbine power coefficient.

Associated to the complexity of 3D effects and flow interactions a first-class mesh becomes essential. Also, one relation between computational time spent and mesh quality was considered.

In spite of this, the simulations were performed with a coarse mesh that in other words translates to a mesh with a reduced number of elements. Therefore, numerical torque values were possible to extract using a function calculator disposed on CFD-post. Table 4.5 shown the data extracted from CFD-post.

Table 4.5: Computed wind turbine torque as a function of the wind speed values.

Wind speed (m/s)	Computed Torque $\times 10^4$(N.m)
6.00	8.80
7.00	11.88
8.00	15.45
10.00	24.06
12.00	34.54
14.00	46.90
16.00	61.19

Computed torque values describe a consistent behavior with the growth of the wind speed values. This behavior was expected due to the increased wind speed be able to consistently produce higher torque values. Furthermore, it can be stated that these torque

values were obtained with the consideration of none resistive element. Therefore, ideally torque values obtained should be higher than those verified in experimental situations.

In short, torque values were achieved in order to evaluate the performance of the rotor. Therefore, following Figure 4.11 shows the power coefficient performance relative to the obtained torque values. Moreover, optimal angular speed values presented in Table 3.4 were used for performing power coefficient calculations.

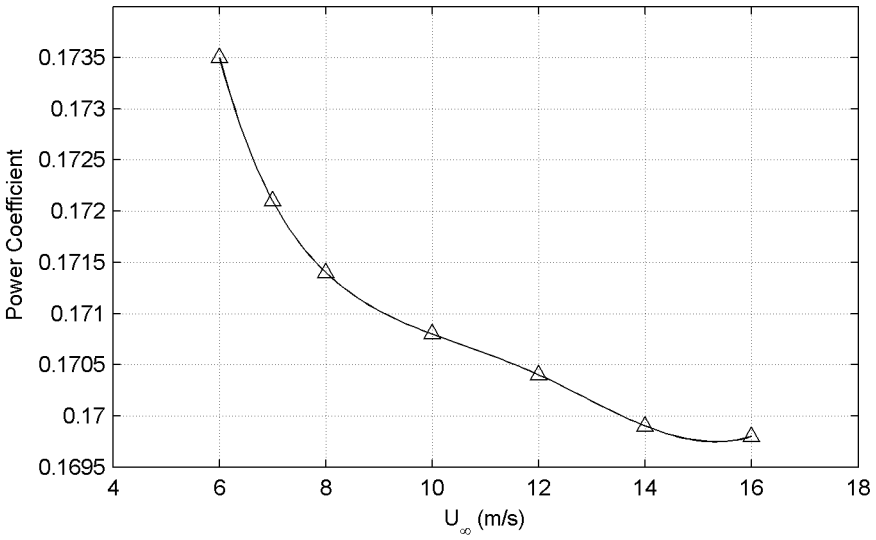

Figure 4.11: Computed wind turbine power coefficient performance as function of different wind speed values.

Figure 4.11 presents a curve that not describe the characteristic power coefficient curve. Data obtained describe a higher performance at lower wind speed values which then gradually decreases the performance, verifying the achievement of lower power coefficient at 16 m/s. In addition, can be stated that the range of wind speed values evaluated was not satisfactory to describe the wind turbine performance.

Nevertheless, CFD calculations were performed to the fluid flow that surrounding the C-D device. Further, flow velocity equal to 6 and 14 m/s were studied.

Figures 4.12 and 4.13 describes the effects that C-D implementation produces in the surrounding air flow, in regarding of 6 and 14 m/s, respectively.

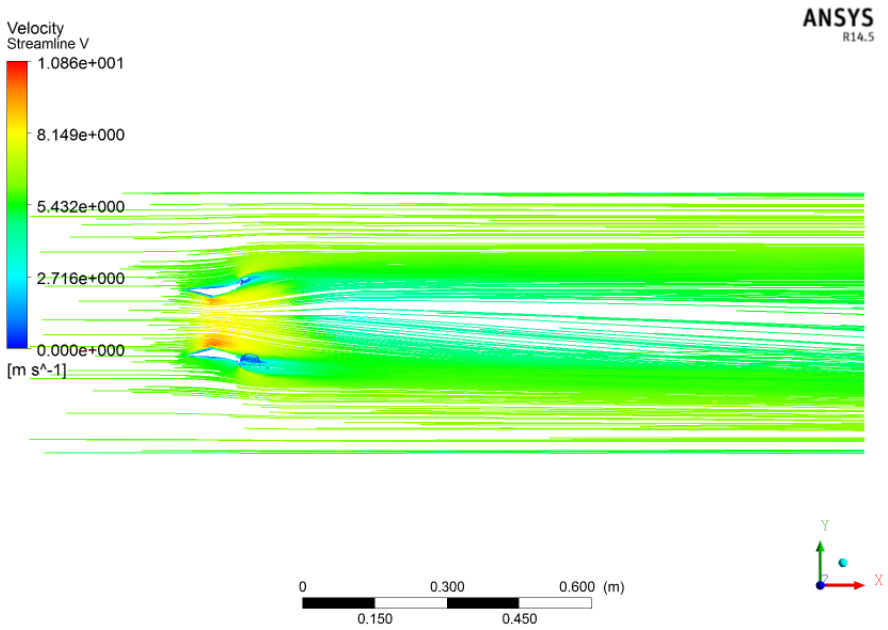

Figure 4.12: Streamline of air flow velocity that surrounds C-D device, considering an approaching wind speed of 6 m/s.

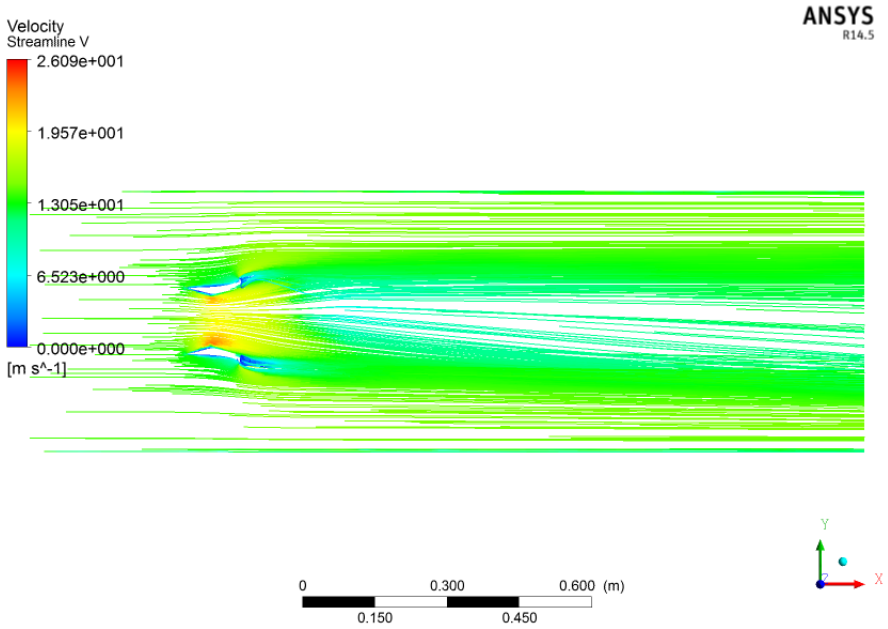

Figure 4.13: Streamline of air flow velocity that surrounds C-D device, considering an approaching wind speed of 14 m/s.

As presented in the previously Figures, C-D generates a somewhat higher velocity values in the zone that wind turbine rotates.

In order to help, the comprehension which occurs in the active area of the wind turbine are presented the Figures 4.14 and 4.15.

Also, with a careful analysis is verified that in the C-D output are generated smaller

vortices that reduce the air flow velocity. Further, this turbulence generated can affect the suction effect that enhances the mass-flow. The vortices generated do not produce significant differences with the air flow velocity increase.

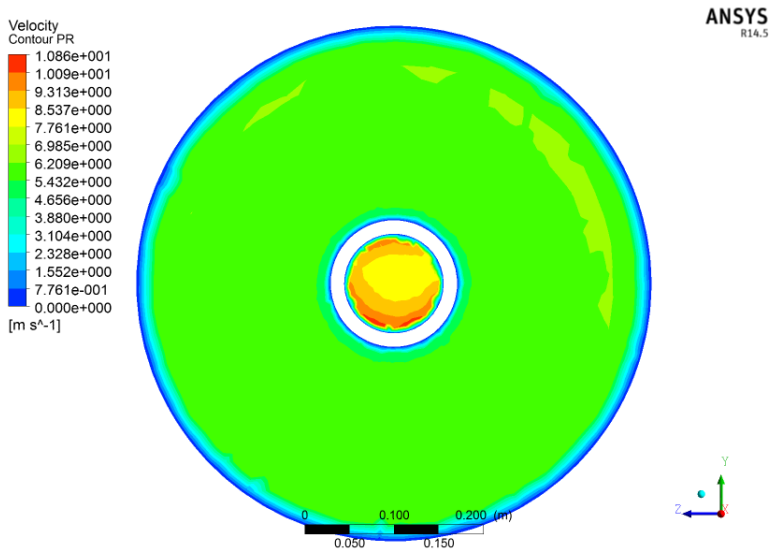

Figure 4.14: Radial contour of velocity experienced at rotor acting zone in C-D device, pondering an approaching wind of 6 m/s.

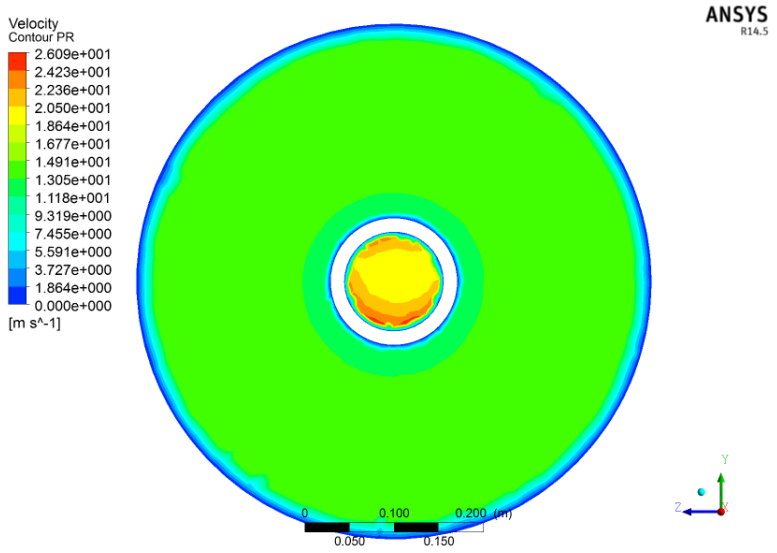

Figure 4.15: Radial contour of velocity experienced at rotor acting zone in C-D device, pondering an approaching wind of 14 m/s.

As C-D exploits the Venturi effect, contours shown in Figures 4.14 and 4.15 are produced to ensure that the reduction of concentrator diameter generates higher velocity values in the wind turbine active zone. These Figures are produced with the consideration of an approaching wind of 6 and 14 m/s, respectively.

Moreover, C-D device produces at a wind of 6 m/s a maximum percentage increase of 81 % and an average increase of 55 %. Relative to the case of 14 m/s one maximum increase of 86 % and an average increase of 60 % are described.

Subsequently, Figures 4.16 and 4.17 are shown to reproduce the turbulence generated at C-D output.

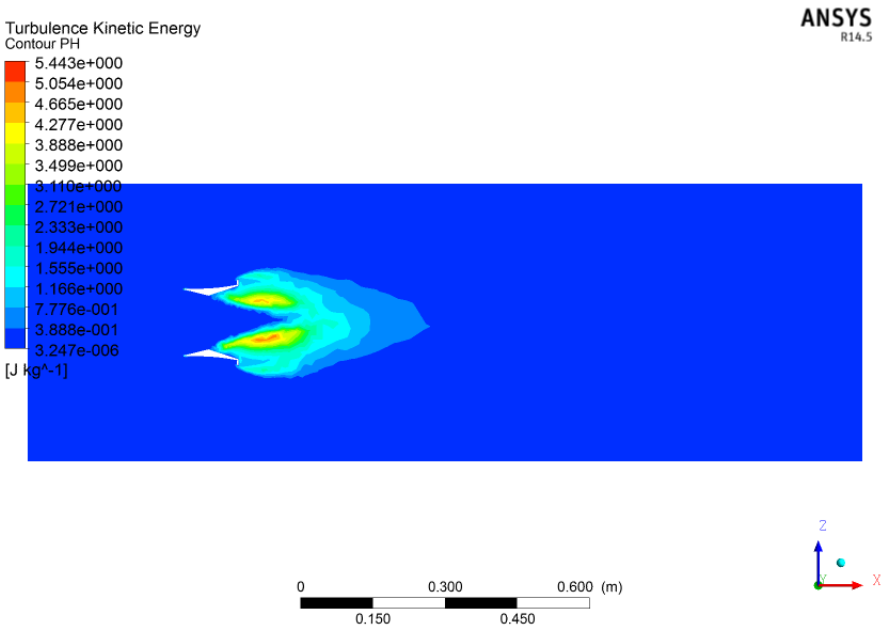

Figure 4.16: Turbulence generated at C-D outflow, evaluated in terms of turbulence kinetic energy, considering an approaching wind of 6 m/s.

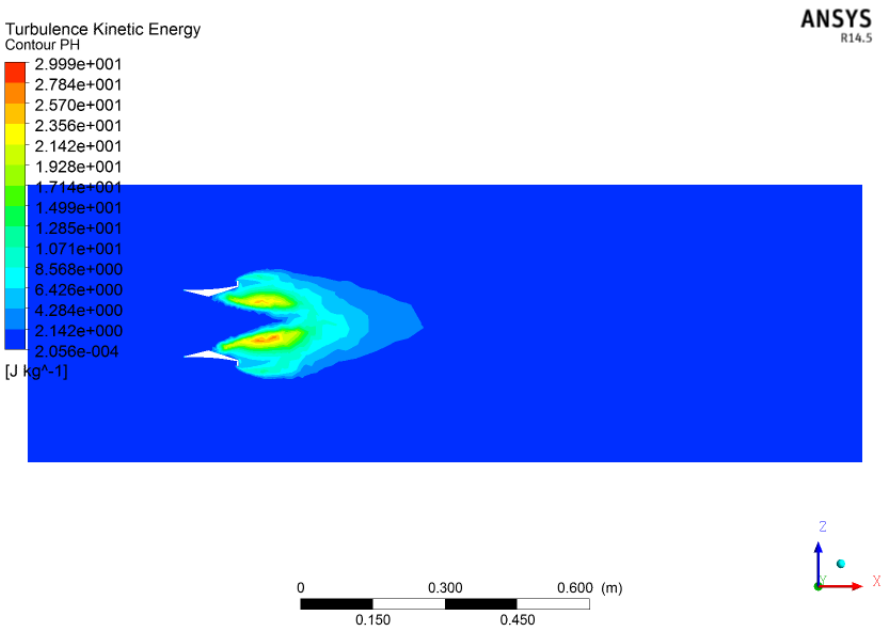

Figure 4.17: Turbulence generated at C-D outflow, evaluated in terms of turbulence kinetic energy, considering an approaching wind of 14 m/s.

Figures presented previously describe a somewhat similar turbulence effects. A more pronounced effect is verified at the inner edge of the diffuser outlet.

In short, diffuser and brim are the fundamentally responsible for this turbulence creation. Moreover, these energy presented in turbulence flow describes enhance with the increment of air flow velocity.

4.3 Experimental vs CFD

In order to study the behavior of drag and lift force, through of the variation attack angle of the wind turbine blade. The two models of wind turbine blade were considered. Numerical results obtained are compared with the available experimental data. Unsteady effects are present in the experimental results and error bars are used to indicate maximum and minimum values obtained. Next Figure 4.18 shows the comparison between experimental results with numerical solution, with main objective to verify the intensity of forces that act on blade.

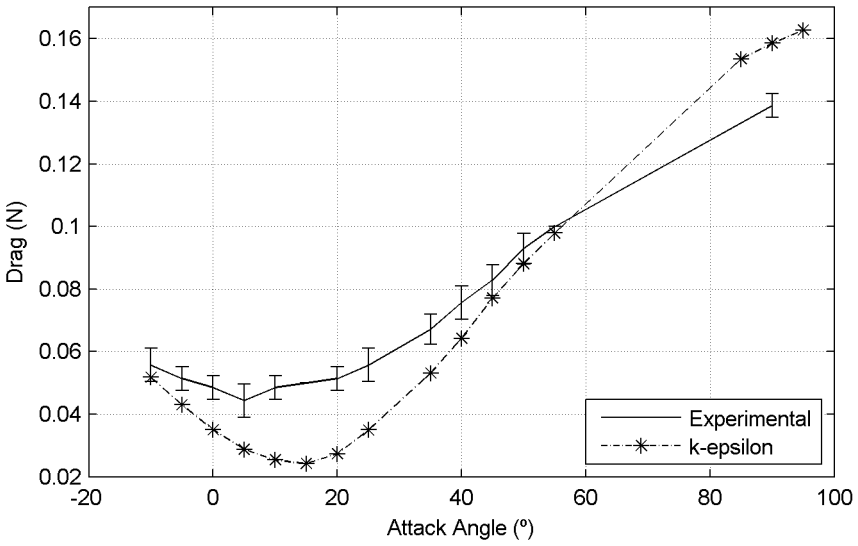

Figure 4.18: Drag force relative to the aerodynamic blade model 1 in function of attack angle variation.

As can be seen from Figure 4.18, results obtained by both methods shown a similar behavior to all attack angle analyzed. Furthermore, for the range of values between 40º - 65º a larger approximation was verified.

Is verified that with increasing the attack angle consequently value of drag force increases. This is occurs due to the increment of projection area blade, perpendicular to flow direction with the variation of attack angle.

Figure 4.19 shows the comparison of experimental results of lift force with numerical solutions, for the same aerodynamic model of wind turbine blade.

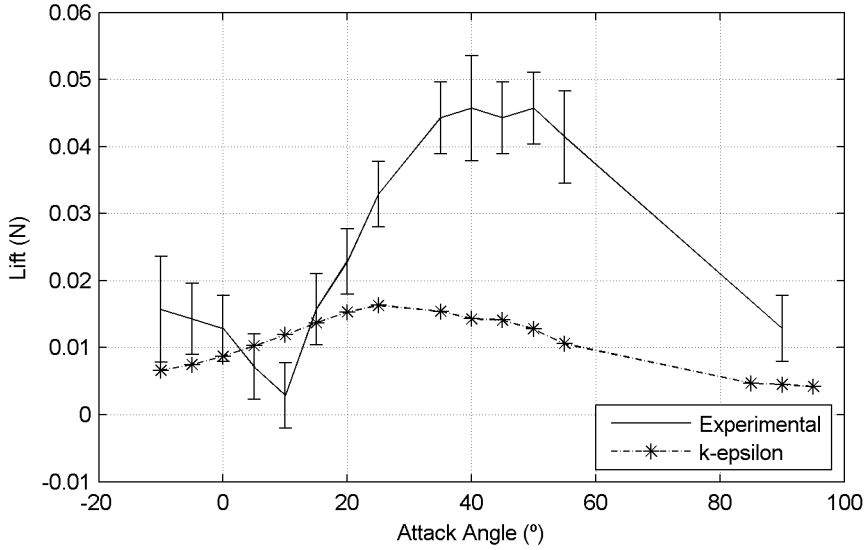

Figure 4.19: Lift force relative to the aerodynamic blade model 1 in function of attack angle variation.

Despite the difference in the peaks maxima corresponding to the experimental a $k-\varepsilon$ results, is observed that the behavior between numerical and experimental method presents some trend. As indicated in Figure 4.19.

Due to a some factors become difficult to study the lift force that act on the blade, such as, the lack of sensitivity of the aerodynamic balance, as well as the small scale of the aerodynamic model, which induces smaller lift force values. These factors help to ensure the difference observed between the intensity of the peaks that both methods produce. A peak maxima lift force, around 0.015 N corresponding to 25º was obtained for $k-\varepsilon$ results. For the case of experimental results was obtained 0.045 N corresponding to an attack angle of around 40º - 50º. Furthermore, beyond the difference in the peaks maxima is observed that these are obtained for different attack angles values.

The second aerodynamic model was considered to improve the results of the forces that act on the blade. This model produce the results presented in Figure 4.20.

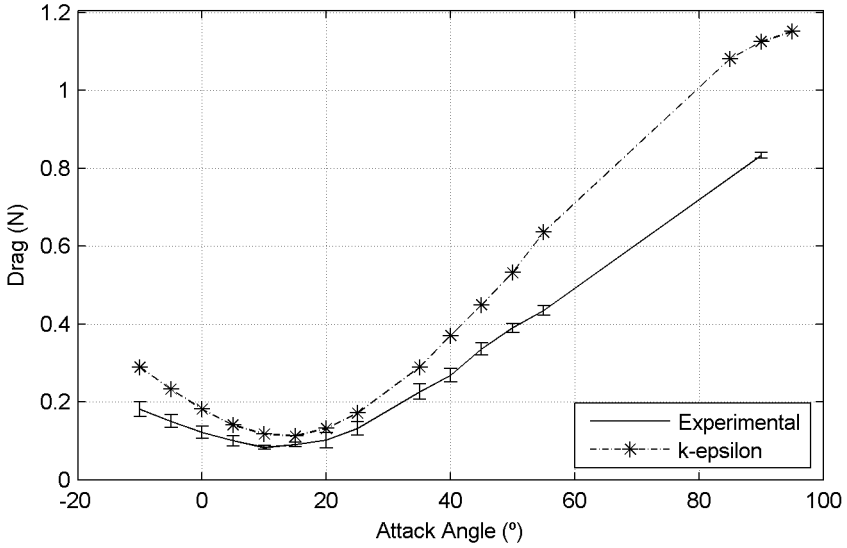

Figure 4.20: Drag force relative to the aerodynamic model blade 2 in function of attack angle variation.

As can be seen in previous figure, through of aerodynamic model 2 is produced a drag force one order of magnitude higher than aerodynamic model 1. Is verified, again, that experimental results show a good approximation to the results obtained in numerical simulations. As can been seen from Figure 4.20 as identified the same behavior observed in Figure 4.18. This behavior describes an increment of the angle attack generates a higher value of drag force. Both aerodynamic models have proved a positively comparison of the experimental results with results obtained in numerical simulations. Due to the approach founded by comparison of both methods is worth noticing that experimental conditions and implementation of computational domain and the structure of turbulence models, that was implemented, were enough factors to obtain a considerable approximation between both methods.

For the case of comparison between both methods to study lift force applied on second aerodynamic model are shown in Figure 4.21.

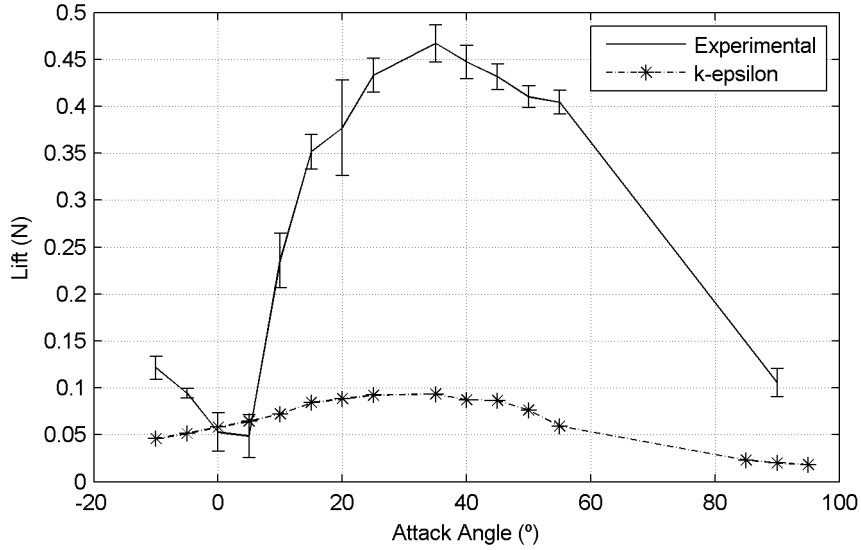

Figure 4.21: Lift force relative to the aerodynamic blade model 2 in function of attack angle variation.

As observed, the aerodynamic model 2 presents the same behavior than aerodynamic model 1. Moreover, this behavior presents again a similar trend but founded some differences in the intensity of the peaks corresponding to the experimental and $k-\varepsilon$ results. The experimental method results in a intensity peak around 0.45 N corresponding to an attack angle of 35º. For the case of $k-\varepsilon$ results was obtained an intensity peak around 0.1 N corresponding to an attack angle around 25º - 35º. Analyzing the results of lift force of both aerodynamic models it's worth noticing that second model generates lift values 100 times greater than the first aerodynamic model, but an inconsistently corresponding to the attack angles was founded. There are some factors responsible by these inconsistently, probably the experimental conditions that are not well defined, our some improvement can be made in numerical simulations, such as an improvement on the grid or adaptation of a different turbulent model.

A clear comparison of these results cannot yet be given based on the available formulation. Probably after testing different turbulence models, or improving the mesh, a better tendency may appear, or other type of evidence which might help in the appreciation of the numerical model performance may appear.

Also wind turbine performance can be compared in terms of the data obtained by experimental trials and numerical simulations. Achieving the computed torque values describes an essential step of numerical method, since without these it would be impractical to evaluate the rotor performance. Since torque values present a somehow importance, in Table 4.6 is performed a clear comparison between the obtained data. Also, is presented the percent variation that may exists between these results.

Table 4.6: Comparison between experimental torque data attained with the numerical torque values in function of wind speed values.

Wind speed (m/s)	Torque $\times 10^4$ (N.m)		Variation (%)
	Experimental	Numerical	
6.00	5.72	8.80	35
7.00	8.15	11.88	31
8.00	9.84	15.45	36
10.00	15.01	24.06	38
12.00	21.51	34.54	38
14.00	26.66	46.90	43
16.00	29.91	61.19	51

As presented in Table 4.6 lower torque values were generated in both situations. Regarding to the relative variation an average variation of approximately 39 % was obtained. These variations reside in the fact that numerical torque data produce higher values relative to experimental data. This behavior it was expected due to the fact that in the numerical method it was not considered any resistive load, thus the rotor rotates as a free body, which is not the case experienced in wind tunnel trials. Experimentally it's considered that the generator is subjected to inertia phenomena, therefore does not rotate as a free body. As described in Table 4.6 the variation probably will continue growing with the wind speed.

In terms of power coefficient performance a clear comparison can be given through a confrontation of the data obtained in both situations. Thus, in Figure 4.22 that comparison is realized.

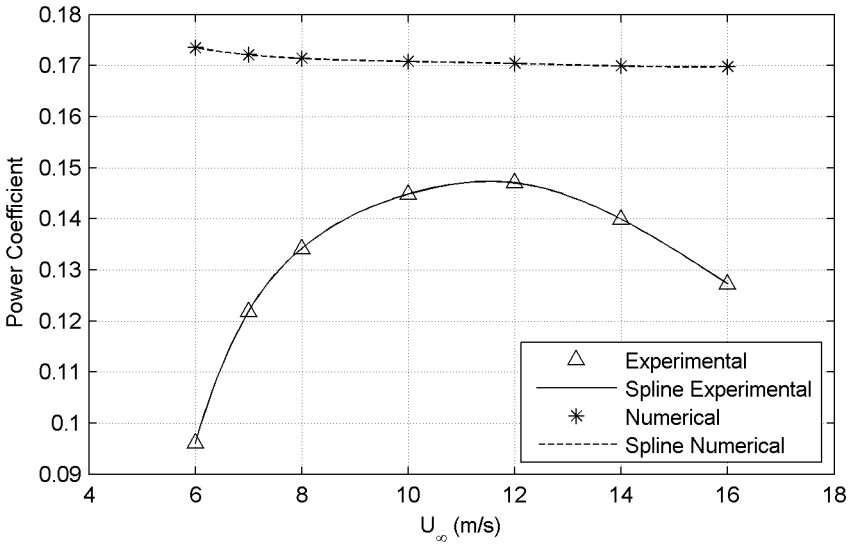

Figure 4.22: Power coefficient confrontation through experimental (△) and numerical (*) data in function wind speed values.

Through, Figure 4.22 it can be stated that the behavior of experimental and numerical data described are not similar. It also can be stated that, numerical curve does not shown the usual bell-shape form that, for example experimental curve presents.

In spite of this, as described in the previous chapters the magnitude of numerical power coefficient values are superior than the experimental power coefficient data. Presently, due to obtaining higher torque values.

Although, the magnitude of the values meets up considerably next to the values obtained experimentally, it can be stated that the numerical methodology applied was not satisfactory due to the fact that was not possible to obtain a performance curve close to the ones obtained experimentally. Therefore, improvements in numerical technique should be applied.

Chapter 5

Conclusions

5.1 Conclusions

In this work, were performed experimental and numerical simulations to an aerodynamic model of a small wind turbine adapted with a Concentrator-Diffuser (C-D). It was evaluated the improvement that this device generates in wind turbine electric production, in terms of power coefficient performance.

Experimental study were performed in a subsonic wind tunnel and at values of approaching wind ranging of 6 to 14 m/s. Relatively to numerical simulations, ANSYS FLUENT was used and was chosen to reproduce the rotor performance and confrontation attempted between the generated values from experimental data.

Also, the aerodynamic performance of a wind turbine blade was evaluated and numerical and experimental simulations were performed testing the behavior of drag and lift force against an attack angle variation. The evaluation was performed for two aerodynamic models presenting different scaling factors

In experimental measurements of wind turbine power performance were attained an increase in the power production, presenting a maximum increase of 120 % and an average improvement of 90 %. This augmentation is more noticeable at lower wind speed values, therefore, the adaptation of one small Wind Turbine with a Concentrator-Diffuser (WT+C-D) turns to be an important synergy. In addition, improvements in power production at zones described by low cut-in speeds can be achieved, offering such benefits for one plausible implementation in urban environments.

Relatively to numerical simulations, preliminary results were obtained. Presented values are relatively to the small wind turbine performance. Preliminary data describes a non-particular similarity with those obtained in experimental tests, were a non-bell-shaped curve was obtained in the performance of power coefficient. In spite of this, was obtained numerical power coefficient values somewhat superior to those relative to experimental trials. Therefore, improvements in numerical methodology must be applied to

reproduce correctly the performance curve described in experimental tests. Moreover, due to these factors, numerical simulations to ensure the wind turbine performance adapting a C-D were not performed. Despite of this, CFD calculations were performed at surrounding air values of 6 m/s and 14 m/s to C-D device. C-D design, at these air flow velocities concluded in a maximum percentage increase of 81 % and an average increase of 55 %. Relative to the case of 14 m/s one maximum increase of 86 % and an average increase of 60 % were attained.

Regarding with of the blade aerodynamic performance lower forces values were generated associated to the reduced size and thickness that blade presents. Experimental and numerical simulation describes a somewhat similar trend. Computed results agree well with experiment, especially for drag forces values.

Efforts in improving the aerodynamic performance of small wind turbines should be encouraged, since the best practices must be implemented in the enhance of the electrical performance of small wind turbines.

5.2 Future Works

- Association of the C-D device with different commercial wind turbines models, implementing experimental and numerical tests;
- Conduct further experiments in the wind tunnel aerodynamic with the upgrade of flow visualizations;
- Application and comparison of Blade Element Theory to perform the calculations of the drag and lift force;
- Comparison of some results with the future field measurements;
- Assessment of the acoustic performance of the wind turbine associated with C-D.

Bibliography

Abe, K., Kihara, H., Sakurai, A., Nishida, M., Ohya, Y., Wada, E. & Sato, K. (2006), 'An experimental study of tip-vortex structures behind a small wind turbine with a flanged diffuser.', *Wind Struct* **9**, 413 – 417.

Abe, K. & Ohya, Y. (2004), 'An investigation of flow fields around flanged diffusers using CFD', *Journal of Wind Engineering and Industrial Aerodynamics* **92**, 315 – 330.

Anderson, J. (2001), *Fundamentals of Aerodynamics*, Anderson Series, third edn, McGraw - Hill Education.

Aranake, A. C., Lakshminarayan, V. K. & Duraisamy (2014), 'Assessment of low-order theories for analysis and design of shrouded wind turbines using CFD', *Journal of Physics: Conference Series* **524**(1), 012077.

Aranake, A. C., Lakshminarayan, V. K. & Duraisamy, K. (2013), Computational analysis of shrouded wind turbine configurations, *in* '51st AIAA Aerospace Sciences Meeting', Dallas.

Armfield (2009), *Data Sheet of Subsonic Wind Tunnel : C2*, Armfield Inc.
URL: *"www.armfield.co.uk/c2"*

Baker, T. J. (2005), 'Mesh generation: Art or science?', *Progress in Aerospace Sciences* **41**(1), 29 – 63.

Balaji, G. & Gnanambal, I. (2014), 'Wind power generator using horizontal axis wind turbine with convergent nozzle', *NISCAIR-CSIR* **73**, 375 – 380.

Bazilevs, Y., Hsu, M.-C., Akkerman, I., Wright, S., Takizawa, K., Henicke, B., Spielman, T. & Tezduyar, T. E. (2011), '3D simulation of wind turbine rotors at full scale. Part I: Geometry modeling and aerodynamics', *International Journal for Numerical Methods in Fluids* **65**(1-3), 207 – 235.

Bern, M. & Plassmann, P. (2000), Mesh generation, *in* 'Handbook of Computational Geometry. Elsevier Science', pp. 291 – 332.

Bet, F. & Grassmann, H. (2003), 'Upgrading conventional wind turbines', *Renewable Energy* **28**(1), 71 – 78.

Betz, A. (1929), 'Energieumsetzungen in venturidusen', *Naturwissenschaften* **17**(10), 160 – 164.

Burkhart, T. A., Andrews, D. M. & Dunning, C. E. (2013), 'Finite element modeling mesh quality, energy balance and validation methods: A review with recommendations associated with the modeling of bone tissue', *Journal of Biomechanics* **46**(9), 1477 – 1488.

Burton, T., Sharpe, D., Jenkins, N. & Bossanyi, E. (2001), *Wind Energy Handbook*, John Wiley & Sons.

Cabezón, D., Migoya, E. & Crespo, A. (2011), 'Comparison of turbulence models for the computational fluid dynamics simulation of wind turbine wakes in the atmospheric boundary layer', *Wind Energy* **14**(7), 909 – 921.

Carcangiu, C. E. (2008), CFD-RANS Study of Horizontal Axis Wind Turbines, PhD thesis, Università degli Studi di Cagliari.

Carroll, J. (2014), Diffuser augmented wind turbine analysis code, Master's thesis, University of Kansas.

Castelli, M. R., Monte, A. D., Quaresimin, M. & Benini, E. (2013), 'Numerical evaluation of aerodynamic and inertial contributions to darrieus wind turbine blade deformation', *Renewable Energy* **51**(0), 101 – 112.

CFD-Wiki (2005). Accessed on June 2014.
URL: *http://www.cfd-online.com*

Chamorro, L. P. & Porté-Agel, F. (2009), 'A wind-tunnel investigation of wind-turbine wakes: Boundary-layer turbulence effects', *Boundary-Layer Meteorology* **132**(1), 129 – 149.

Chen, Y. (2011), A Study of the Aerodynamic Behavior of a NREL Phase VI Wind Turbine Using the CFD Methodology, PhD thesis, Wright State University, Wright State University.

de Vries, O. (1979), *Fluid Dynamic Aspects of Wind Energy Conversion*, AGARD.

Digraskar, D. (2010), Simulations of flow over wind turbines, Master's thesis, University of Massachusetts.

Eggleston, D. M. & Stoddard, F. S. (1987), *Wind turbine engineering design*, Van Nostrand Reinhold.

Ferziger, J. H. & Peric, M. (2002), *Computational Method for Fluid Dynamics*, third edn, Springer-Verlag.

Fleck, G. D. (2012), Simulação de grandes escalas para análise numérica da esteira aerodinâmica da turbina eólica NREL UAE phase VI, Master's thesis, Universidade Federal do Rio Grande do Sul.

Fluent (2005), *Fluent 6.2 Documentation - Modeling Turbulence*.

Fluent (2011*a*), *ANSYS FLUENT 14.0 Documentation*, ANSYS, Inc.

Fluent (2011*b*), *ANSYS FLUENT Theory Guide*, ANSYS, Inc.

García-Abril, H. J. L. (2014), Estudio y optimización de diseño de un concentrador-difusor para un aerogenerador de baja potencia, Master's thesis, Instituto Politécnico de Bragança.

Gilbert, B. L. & Foreman, K. (1979), 'Experimental demonstration of the diffuser-augmented wind turbine concept', *Journal of Energy* **3**(4), 235 – 240.

Gilbert, B. L. & Foreman, K. M. (1983), 'Experiments with a diffuser-augmented model wind turbine', *Journal of Energy Resources Technology* **105**(1), 46 – 53.

Gomis, L. L. (2011), Effect of diffuser augmented micro wind turbines features on device performance, Master's thesis, School of Mechanical, Materials and Mechatronics Engineering, University of Wollongong.

Grassmann, H., Bet, F., Cabras, G., Ceschia, M., Cobai, D. & DelPapa, C. (2003), 'A partially static turbine - first experimental results', *Renewable Energy* **28**(11), 1779 – 1785.

Hau, E. (2006), *Wind Turbines - Fundamentals, Technologies, Application, Economics*, second edn, Springer.

Hjort, S. & Larsen, H. (2014), 'A multi-element diffuser augmented wind turbine', *Energies* **7**(5), 3256 – 3281.

Igra, O. (1981), 'Research and development for shrouded wind turbines', *Energy Conversion and Management* **21**(1), 13 – 48.

Jafari, S. & Kosasih, B. (2014), 'Flow analysis of shrouded small wind turbine with a simple frustum diffuser with computational fluid dynamics simulations', *Journal of Wind Engineering and Industrial Aerodynamics* **125**(0), 102 – 110.

Jamieson, P. (2008), Beating betz-energy extraction limits in a uniform flow field, *in* 'Garrad Hassan and Partners', EWEA, Brussels, Belgium.

Jonkman, J. M. (2003), Modeling of the UAE wind turbine for refinem FAST-AD, Technical Report NREL/TP-500-34755, National Renewable Energy Laboratory.

Kardous, M., Chaker, R., Aloui, F. & Nasrallah, S. (2013), 'On the dependence of an empty flanged diffuser performance on flange height: Numerical simulations and {PIV} visualizations', *Renewable Energy* **56**(0), 123 – 128. The International Conference on Renewable Energy: Generation and Applications.

Knupp, P. (2007), Remarks on mesh quality, *in* '45th AIAA Aerospace Sciences Meeting and Exhibit', American Institute of Aeronautics and Astronautics, pp. –.

Kogan, A. & Seginer, A. (1963), Shrouded aerogenerator design study II, axisymmetircal shroud performance, *in* 'Proceedings of the Fifth Israel Annual Conference on Aviation and Astronautics', Israel.

Kosasih, B. & Tondelli, A. (2012), 'Experimental study of shrouded micro-wind turbine', *Procedia Engineering* **49**(0), 92 – 98. International Energy Congress 2012.

Krogstad, P. & Eriksen, P. E. (2013), '"blind test" calculations of the performance and wake development for a model wind turbine', *Renewable Energy* **50**(0), 325 – 333.

Kulunk, E. (2011), *Aerodynamics of Wind Turbines, Fundamentals and Advanced Topics in Wind Power*, InTech.

Lanzafame, R., Mauro, S. & Messina, M. (2013), 'Wind turbine CFD modeling using a correlation-based transitional model', *Renewable Energy* **52**(0), 31 – 39.

Launder, B. E. & Spalding, D. B. (1972), *Lectures in Mathematical Models of Turbulence*, Academic Press, London, England.

Lilley, G. M., Rainbird, W. J. & Association, E. R. (1956), *A Preliminary Report on the Design and Performance of Ducted Windmills*, CoA report aero, College of Aeronautics.

Makridis, A. & Chick, J. (2013), 'Validation of a CFD model of wind turbine wakes with terrain effects', *Journal of Wind Engineering and Industrial Aerodynamics* **123, Part A**(0), 12 – 29.

Mansour, K. & Meskinkhoda, P. (2014), 'Computational analysis of flow fields around flanged diffusers', *Journal of Wind Engineering and Industrial Aerodynamics* **124**(0), 109 – 120.

Manwell, J. F., McGowan, J. G. & Rogers, A. L. (2002), *Wind Energy Explained: Theory, Design and Application*, Wiley.

Massey, B. S. (1996), *Mechanics of fluids*, 6ª edn, Chapman & Hall, London.

Mo, J. O., Choudhry, A., Arjomandi, M. & Lee, Y. (2013), 'Large eddy simulation of the wind turbine wake characteristics in the numerical wind tunnel model', *Journal of Wind Engineering and Industrial Aerodynamics* **112**(0), 11 – 24.

Moshfeghi, M., Song, Y. J. & Xie, Y. H. (2012), 'Effects of near-wall grid spacing on SST-K-W model using NREL phase VI horizontal axis wind turbine', *Journal of Wind Engineering and Industrial Aerodynamics* **107 - 108**(0), 94 – 105.

Ohya, Y. & Karasudani, T. (2010), 'A shrouded wind turbine generating high output power with wind-lens technology', *Energies* **3**(4), 634 – 649.

Ohya, Y., Karasudani, T., Sakurai, A., Abe, K. & Inoue, M. (2008), 'Development of a shrouded wind turbine with a flanged diffuser', *Journal of Wind Engineering and Industrial Aerodynamics* **96**(5), 524 – 539.

Oliveira, L. & Lopes, A. (2012), *Mecânica dos Fluidos*, 4 edn, LIDEL.

Paulo, J. A. R. (2013), Construção, desenvolvimento e otimização de concentrador e difusor para turbina eólica, Master's thesis, Escola Superior de Tecnologia e Gestão : Instituito Politécnico de Bragança.

Phillips, D. G. (2003), An Investigation on Diffuser Augmented Wind Turbine Design, PhD thesis, University of Auckland.

Rashford, B. S., Macsalka, N. & Geiger, M. (2010), 'The effect of altitude on small wind turbine power production'.

Reynolds, O. (1883), 'An experimental investigation of the circumstances which determine whether the motion of water shall be direct or sinuous, and of the law of resistance in parallel channels.', *Philosophical Tra* **174**, 935–982.

Ribeiro, L. M. F., Paulo, J. A. R. & Garcia, V. (2013), Convergent-diffuser for small horizontal wind turbines, *in* 'AWEA - Windpower conference e exhibition', Chicago.

Sargsyan, A. (2010), Simulation and modeling of flow field around a horizontal axis wind turbine (HAWT) using RANS method by Armen Sargsyan, Master's thesis, Florida Atlantic University.

Schlichting, H. (1979), *Boundary-Layer Theory*, Physic and astronomy, seventh edn, MacGraw - Hill.

Shih, T., Liou, W. W., Shabbir, A., Yang, Z. & Zhu, J. (1995), 'A new k-epsilon eddy viscosity model for high Reynolds number turbulent flows', *Computers & Fluids* **24**(3), 227 – 238.

Shives, M. & Crawford, C. (2010), Computational analysis of ducted turbine performance, *in* 'Third International Conference on Ocean Energy', Bilbao.

Stokes, G. G. (1851), 'On the Effect of the Internal Friction of Fluids on the Motion of Pendulums', *Transactions of the Cambridge Philosophical Society* **9**, 8.

Sumner, J., Watters, C. S. & Masson, C. (2010), 'CFD in wind energy: The virtual, multiscale wind tunnel', *Energies* **3**(5), 989 – 1013.

Takahashi, S., Hata, Y., Ohya, Y., Karasudani, T. & Uchida, T. (2012), 'Behavior of the blade tip vortices of a wind turbine equipped with a brimmed-diffuser shroud', *Energies* **5**(12), 5229 – 5242.

Ten Hoopen, P. D. C. (2009), An experimental and computational investigation of a diffuser augmented wind turbine, Master's thesis, Delft University of Technology.

Toshimitsu, K., Nishikawa, K., Haruki, W., Oono, S., Takao, M. & Ohya, Y. (2008), 'PIV measurements of flows around the wind turbines with a flanged-diffuser shroud', *Journal of Thermal Science* **17**(4), 375 – 380.

Trias, F. X. & Lehmkuhl, O. (2011), 'A Self-Adaptive Strategy For The Time Integration Of Navier-Stokes Equations', *Numerical Heat Transfer Part B-Fundamentals* **60**(2), 116 – 134.

Van Bussel, G. J. W. (2007), 'The science of making more torque from wind: Diffuser experiments and theory revisited.', *Journal of Physics: Conference Series* **75**(1), 012010.

Vaz, D. A. T. D. R., Mesquita, A. L. A., Vaz, J. R. P., Blanco, C. J. C. & Pinho, J. T. (2014), 'An extension of the blade element momentum method applied to diffuser augmented wind turbines', *Energy Conversion and Management* **n/a**(0), n/a – n/a.

Vennard, J. K., Street, R. L. & Watters, G. Z. (1996), *Elementary Fluid Mechanics:*, seventh edn, John Wiley & Sons.

Versteeg, H. & Malalasekera, W. (2007), *An Introduction to Computational Fluid Dynamics: The Finite Volume Method (2nd Edition)*, 2 edn, Prentice Hall.

Wang, F., Bai, L., Fletcher, J., Whiteford, J. & Cullen, D. (2008), 'The methodology for aerodynamic study on a small domestic wind turbine with scoop', *Journal of Wind Engineering and Industrial Aerodynamics* **96**(1), 1 – 24.

White, F. M. (1998), *Fluid Mechanics*, fourth edn, McGraw-Hill Series.

Wilcox, D. C. (1994), *Turbulence Modeling for CFD*, second edn, DCW Industries, La Canada, California.

Wilson, R. E. & Lissaman, P. B. S. (1974), *Applied Aerodynamics of Wind Power Machines*, Oregon State University, Corvallis, Oregon.